

# Clustering in Hilbert simplex geometry

Frank Nielsen\* Ke Sun†

## Abstract

Clustering categorical distributions in the probability simplex is a fundamental task met in many applications dealing with normalized histograms. Traditionally, the differential-geometric structures of the probability simplex have been used either by (i) setting the Riemannian metric tensor to the Fisher information matrix of the categorical distributions, or (ii) defining the dualistic information-geometric structure induced by a smooth dissimilarity measure, the Kullback-Leibler divergence. In this work, we introduce for this clustering task a novel computationally-friendly framework for modeling the probability simplex termed *Hilbert simplex geometry*. In the Hilbert simplex geometry, the distance function is described by a polytope. We discuss the pros and cons of those different statistical modelings, and benchmark experimentally these geometries for center-based  $k$ -means and  $k$ -center clusterings. We show that Hilbert metric in the probability simplex satisfies the property of information monotonicity. Furthermore, since a canonical Hilbert metric distance can be defined on any bounded convex subset of the Euclidean space, we also consider Hilbert’s projective geometry of the ellipope of correlation matrices and study its clustering performances.

**Keywords:** Fisher-Riemannian geometry, information geometry, Finsler geometry, information monotonicity, multinoulli distribution, Hilbert simplex geometry, Birkhoff cone metric, variation norm, polytope distance, ellipope, Thompson metric,  $k$ -means clustering,  $k$ -center clustering.

## 1 Introduction and motivation

The categorical distributions and multinomial distributions are important probability distributions often met in data analysis [3], text mining [2], computer vision [51] and machine learning [52]. A multinomial distribution over a set  $\mathcal{X} = \{e_0, \dots, e_d\}$  of outcomes (e.g., the  $d+1$  distinct colored faces of a die) is defined as follows: Let  $\lambda_p^i > 0$  denote the probability that outcome  $e_i$  occurs for  $i \in \{0, \dots, d\}$  (with  $\sum_{i=0}^d \lambda_p^i = 1$ ). Denote by  $m$  the total number of events, with  $m_i$  reporting the number of outcome  $e_i$ . Then the probability  $\Pr(X_0 = m_0, \dots, X_d = m_d)$  that a multinomial random variable  $X = (X_0, \dots, X_d) \sim \text{Mult}(p = (\lambda_p^0, \dots, \lambda_p^d), m)$  (where  $X_i$  count the number of events  $e_i$ , and  $\sum_{i=0}^d m_i = m$ ) is given by the following probability mass function (pmf):

$$\Pr(X_0 = m_0, \dots, X_d = m_d) = \frac{m!}{\prod_{i=0}^d m_i!} \prod_{i=0}^d (\lambda_p^i)^{m_i}.$$

The multinomial distribution is called a binomial distribution when  $d = 1$  (e.g., coin tossing), a Bernoulli distribution when  $m = 1$ , and a “multinoulli distribution” (or categorical distribution) when  $m = 1$  and  $d > 1$ . The multinomial distribution is also called a generalized Bernoulli distribution. A random variable  $X$  following a multinoulli distribution is denoted by  $X = (X_0, \dots, X_d) \sim \text{Mult}(p = (\lambda_p^0, \dots, \lambda_p^d))$ . The multinomial/multinoulli distribution provides an important *feature representation* in machine learning that is often met in applications [45, 74, 26] as normalized histograms (with non-empty bins) as illustrated in Figure 1.

A multinomial distribution  $p \in \Delta^d$  can be thought as a point lying in the probability simplex  $\Delta^d$  (standard simplex) with coordinates  $p = (\lambda_p^0, \dots, \lambda_p^d)$  such that  $\lambda_p^i = \Pr(X = e_i) > 0$  and  $\sum_{i=0}^d \lambda_p^i = 1$ . The open probability simplex  $\Delta^d$  can be embedded in  $\mathbb{R}^{d+1}$  on the hyperplane  $H_{\Delta^d} : \sum_{i=0}^d x^i = 1$ . Notice that observations with  $D$  categorical

---

\*Sony Computer Science Laboratories, Tokyo, Japan, Frank.Nielsen@acm.org

†CSIRO Data61, Sydney, Australia, Ke.Sun@data61.csiro.au

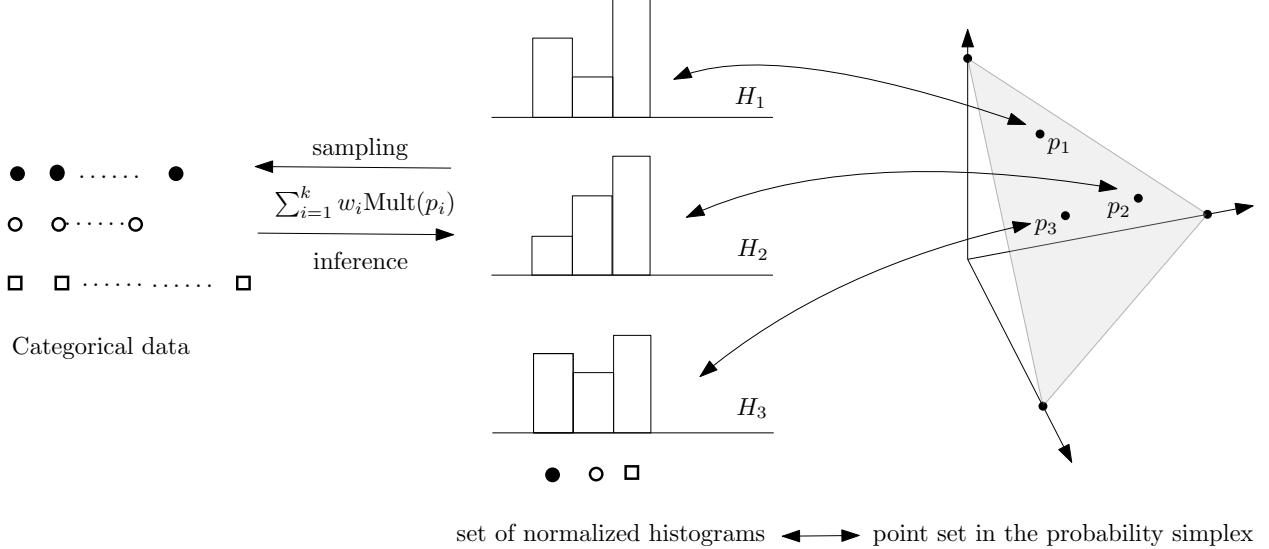


Figure 1: Categorical datasets modeled by a generative statistical mixture model of multinoulli distributions can be visualized as a weighted set of normalized histograms or equivalently by a weighted point set encoding multinoulli distributions in the probability simplex  $\Delta^d$  (here,  $d = 2$  for trinoulli distributions — trinomial distributions with a single trial).

attributes can be clustered using  $k$ -mode [38] with respect to the Hamming distance. Here, we consider the different task of clustering a set  $\Lambda = \{p_1, \dots, p_n\}$  of  $n$  categorical/multinomial distributions in  $\Delta^d$  [26] using center-based  $k$ -means++ or  $k$ -center clustering algorithms [8, 34], which rely on a dissimilarity measure (loosely called distance or divergence when smooth) between any two categorical distributions. In this work, we mainly consider four distances with their underlying geometries: (1) Fisher-Hotelling-Rao distance  $\rho_{FHR}$  (spherical geometry), (2) Kullback-Leibler divergence  $\rho_{KL}$  (dually flat geometry), (3) Hilbert distance  $\rho_{HG}$  (generalize Klein's hyperbolic geometry), and (4) the total variation/L1 distance (norm geometry). The geometric structures of spaces are necessary in algorithms, for example, to define midpoint distributions. Figure 2 displays the  $k$ -center clustering results obtained with these four geometries as well as the  $L^1$  distance  $\rho_{L1}$  normed geometry on toy synthetic datasets in  $\Delta^2$ . We shall now explain the Hilbert simplex geometry applied to the probability simplex, describe how to perform  $k$ -center clustering in Hilbert geometry, and report experimental results that demonstrate the superiority of the Hilbert geometry when clustering multinomials and correlation matrices.

The rest of this paper is organized as follows: Section 2 formally introduces the distance measures in  $\Delta^d$ . Section 3 introduces how to efficiently compute the Hilbert distance, and prove that Hilbert simplex distance satisfies the information monotonicity (in §3.3). Section 4 presents algorithms for Hilbert minimax centers and Hilbert center-based clustering. Section 5 performs an empirical study of clustering multinomial distributions, comparing Riemannian geometry, information geometry, and Hilbert geometry. Section 6 presents a second use case of Hilbert geometry in machine learning: clustering correlation matrices in the ellipope [81]. Finally, section 7 concludes this work by summarizing the pros and cons of each geometry. Although some contents require prior knowledge on geometric structures, we will present the detailed algorithms so that the general audience can still benefit from this work.

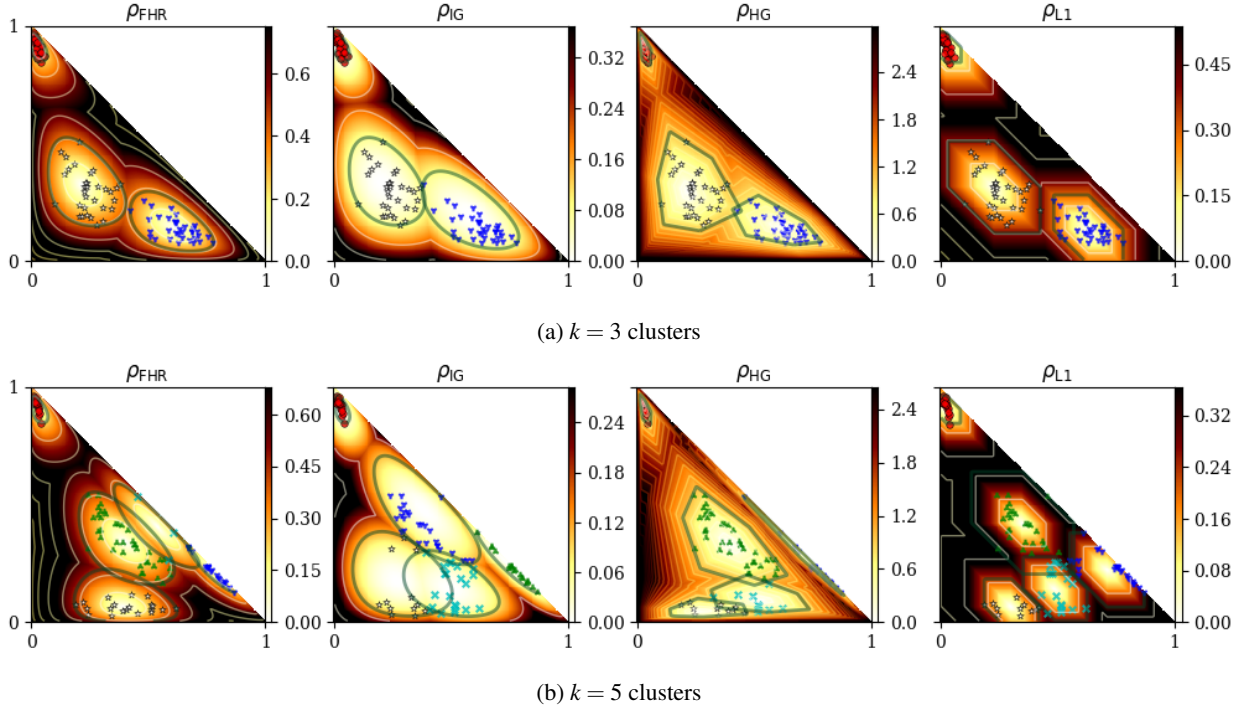


Figure 2: Visualizing some  $k$ -center clustering results on a toy dataset in the space of trinomials  $\Delta^2$  for the considered four types of distances (and underlying geometries): Fisher-Hotelling-Rao metric distance (Riemannian geometry), Kullback-Leibler non-metric divergence (information geometry), Hilbert metric distance (Hilbert projective geometry), and total variation/ $L_1$  metric distance (norm geometry). Observe that the  $L_1$  balls have hexagonal shapes on the probability simplex (intersection of a rotated cube with the plane  $H_{\Delta^d}$ ). The color density maps indicate the distance from any point to its nearest cluster center.

## 2 Four distances with their underlying geometries

### 2.1 Fisher-Hotelling-Rao Riemannian geometry

The Rao distance between two multinomial distributions is [41, 45]:

$$\rho_{\text{FHR}}(p, q) = 2 \arccos \left( \sum_{i=0}^d \sqrt{\lambda_p^i \lambda_q^i} \right). \quad (1)$$

It is a Riemannian metric length distance (satisfying the symmetric and triangular inequality axioms) obtained by setting the metric tensor  $g$  to the *Fisher information matrix* (FIM)  $\mathcal{I}(p) = (g_{ij}(p))_{d \times d}$  with respect to the coordinate system  $(\lambda_p^1, \dots, \lambda_p^d)$ , where

$$g_{ij}(p) = \frac{\delta_{ij}}{\lambda_p^i} + \frac{1}{\lambda_p^0}.$$

We term this geometry the *Fisher-Hotelling-Rao (FHR) geometry* [37, 79, 70, 71]. The metric tensor  $g$  allows one to define an inner product on each tangent plane  $T_p$  of the probability simplex manifold:  $\langle u, v \rangle_p = u^\top g(p)v$ . When  $g$  is everywhere the identity matrix, we recover the Euclidean (Riemannian) geometry with the inner product being the scalar product:  $\langle u, v \rangle = u^\top v$ . The geodesics  $\gamma(p, q; \alpha)$  are defined by the Levi-Civita metric connection [4, 22] that is derived from the metric tensor. The FHR manifold can be embedded in the positive orthant of an Euclidean  $d$ -sphere in  $\mathbb{R}^{d+1}$  by using the *square root representation*  $\lambda \mapsto \sqrt{\lambda}$  [41]. Therefore the FHR manifold modeling of

$\Delta^d$  has constant *positive* curvature: It is a spherical geometry restricted to the positive orthant with the metric distance measuring the arc length on a great circle.

## 2.2 Information geometry

A divergence  $D$  is a smooth  $C^3$  differentiable dissimilarity measure [5] that allows to define a dual structure in Information Geometry (IG), see [78, 22, 4]. A  $f$ -divergence is defined for a strictly convex function  $f$  with  $f(1) = 0$  by:

$$I_f(p : q) = \sum_{i=0}^d \lambda_p^i f\left(\frac{\lambda_q^i}{\lambda_p^i}\right) \geq f(1) = 0.$$

It is a *separable* divergence since the  $d$ -variate divergence can be written as a sum of  $d$  univariate (scalar) divergences:  $I_f(p : q) = \sum_{i=0}^d I_f(\lambda_p^i : \lambda_q^i)$ . The class of  $f$ -divergences plays an essential role in information theory since they are provably the *only* separable divergences that satisfy the *information monotonicity* property [4, 49] (for  $d \geq 2$ ). That is, by coarse-graining the histograms, we obtain lower-dimensional multinomials, say  $p'$  and  $q'$ , such that  $0 \leq I_f(p' : q') \leq I_f(p : q)$  [4]. The Kullback-Leibler (KL) divergence  $\rho_{\text{IG}}$  is a  $f$ -divergence obtained for the functional generator  $f(u) = -\log u$ :

$$\rho_{\text{IG}}(p, q) = \sum_{i=0}^d \lambda_p^i \log \frac{\lambda_p^i}{\lambda_q^i}. \quad (2)$$

It is an asymmetric non-metric distance:  $\rho_{\text{IG}}(p, q) \neq \rho_{\text{IG}}(q, p)$ . In differential geometry, the structure of a manifold is defined by two independent components:

1. A *metric tensor*  $g$  that allows to define an inner product  $\langle \cdot, \cdot \rangle_p$  at each tangent space (for measuring vector lengths and angles between vectors);
2. A *connection*  $\nabla$  that defines *parallel transport*  $\Pi_c^\nabla$ , *i.e.*, a way to move a tangent vector from one tangent plane  $T_p$  to any other one  $T_q$  along a smooth curve  $c$ , with  $c(0) = p$  and  $c(1) = q$ .

In FHR geometry, the implicitly-used connection is called the Levi-Civita connection that is induced by the metric  $g$ :  $\nabla^{\text{LC}} = \nabla(g)$ . It is a metric connection since it ensures that  $\langle u, v \rangle_p = \langle \Pi_{c(t)}^{\nabla^{\text{LC}}} u, \Pi_{c(t)}^{\nabla^{\text{LC}}} v \rangle_{c(t)}$  for  $t \in [0, 1]$ . The underlying information-geometric structure of KL is characterized by a pair of *dual* connections [4]  $\nabla = \nabla^{(-1)}$  (mixture connection) and  $\nabla^* = \nabla^{(1)}$  (exponential connection) that induces a corresponding pair of dual geodesics (technically,  $\pm 1$ -autoparallel curves, [22]). Those connections are said *flat* as they define two dual global affine coordinate systems  $\theta$  and  $\eta$  on which the  $\theta$ - and  $\eta$ -geodesics are (Euclidean) straight line segments, respectively. For multinomials, the *expectation parameters* are:  $\eta = (\lambda^1, \dots, \lambda^d)$  and they one-to-one correspond to the *natural parameters*:

$\theta = \left( \log \frac{\lambda^1}{\lambda^0}, \dots, \log \frac{\lambda^d}{\lambda^0} \right) \in \mathbb{R}^d$ . Thus in IG, we have two kinds of midpoint multinomials of  $p$  and  $q$ , depending on whether we perform the (linear) interpolation on the  $\theta$ - or the  $\eta$ -geodesics. Informally speaking, the dual connections  $\nabla^{(\pm 1)}$  are said coupled to the FIM since we have  $\frac{\nabla + \nabla^*}{2} = \nabla(g) = \nabla^{\text{LC}}$ . Those dual (torsion-free affine) connections are not metric connections but enjoy the following metric-compatibility property when used together as follows:  $\langle u, v \rangle_p = \langle \Pi_{c(t)} u, \Pi_{c(t)}^* v \rangle_{c(t)}$  (for  $t \in [0, 1]$ ), where  $\Pi := \Pi^\nabla$  and  $\Pi^* := \Pi^{\nabla^*}$  are the corresponding induced dual parallel transports. The geometry of  $f$ -divergences [5] is the  $\alpha$ -geometry (for  $\alpha = 3 + 2f'''(1)$ ) with the dual  $\pm \alpha$ -connections, where  $\nabla^{(\alpha)} = \frac{1+\alpha}{2} \nabla^* + \frac{1-\alpha}{2} \nabla$ . The Levi-Civita metric connection is  $\nabla^{\text{LC}} = \nabla^{(0)}$ . More generally, it was shown how to build a dual information-geometric structure for *any* divergence [5]. For example, we can build a dual structure from the symmetric Cauchy-Schwarz divergence [39]:

$$\rho_{\text{CS}}(p, q) = -\log \frac{\langle \lambda_p, \lambda_q \rangle}{\sqrt{\langle \lambda_p, \lambda_p \rangle \langle \lambda_q, \lambda_q \rangle}}. \quad (3)$$

## 2.3 Hilbert simplex geometry

In Hilbert geometry (HG), we are given a bounded convex domain  $\mathcal{C}$  (here,  $\mathcal{C} = \Delta^d$ ), and the distance between any two points  $M, M'$  of  $\mathcal{C}$  is defined [36] as follows: Consider the two intersection points  $AA'$  of the line  $(MM')$  with  $\mathcal{C}$ ,

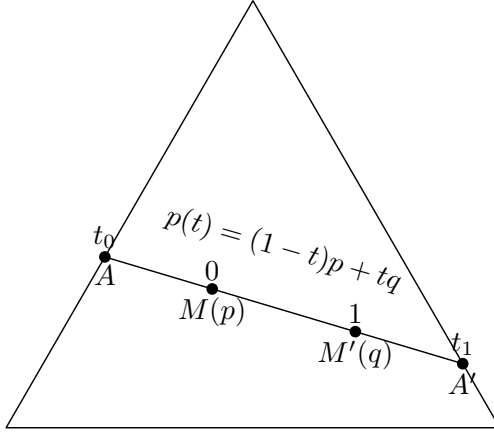


Figure 3: Computing the Hilbert metric distance for trinomials on the 2D probability simplex as the logarithm of the cross ratio  $(M, M'; A, A')$  of the four collinear points  $A, M, M'$  and  $A'$ .

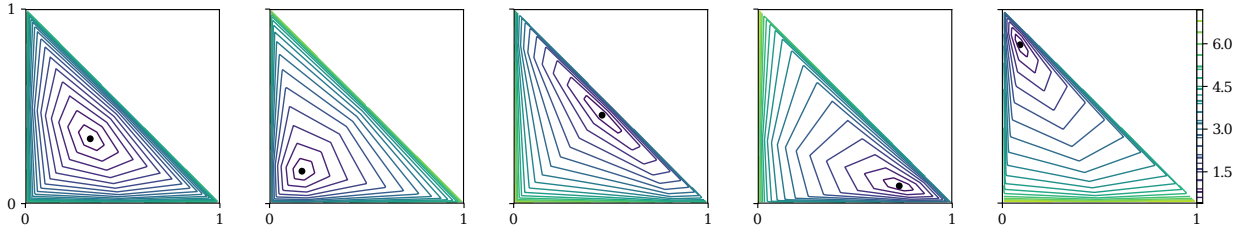


Figure 4: Balls in the Hilbert simplex geometry  $\Delta^2$  have polygonal Euclidean shapes of constant combinatorial complexity. At infinitesimal scale, the balls have hexagonal shapes, showing that the Hilbert geometry is not Riemannian.

and order them on the line so that we have  $A, M, M', A'$ . Then the Hilbert metric distance [19] is defined by:

$$\rho_{\text{HG}}(M, M') = \begin{cases} \left| \log \frac{|A'M||AM'|}{|A'M'||AM|} \right|, & M \neq M', \\ 0 & M = M'. \end{cases} \quad (4)$$

It is also called the Hilbert cross-ratio metric distance [28, 46]. Notice that we take the absolute value of the logarithm since the Hilbert distance is a *signed distance* [73]. When  $\mathcal{C}$  is the unit ball, HG lets us recover the Klein hyperbolic geometry [46]. When  $\mathcal{C}$  is a quadric bounded convex domain, we obtain the Cayley-Klein hyperbolic geometry [15] which can be studied with the Riemannian structure and the corresponding metric distance called the curved Mahalanobis distances [56, 55]. Cayley-Klein hyperbolic geometries have negative curvature. Elements on the boundary are called ideal elements [80].

In Hilbert geometry, the geodesics are *straight* Euclidean lines making them convenient for computation. Furthermore, the domain boundary  $\partial\mathcal{C}$  needs not to be smooth: One may also consider bounded polytopes [14]. This is particularly interesting for modeling  $\Delta^d$ , the  $d$ -dimensional open standard simplex. We call this geometry the *Hilbert simplex geometry* [64]. In Figure 3, we show that the Hilbert distance between two multinomial distributions  $p$  ( $M$ ) and  $q$  ( $M'$ ) can be computed by finding the two intersection points of the line  $(1-t)p + tq$  with  $\partial\Delta^d$ , denoted as  $t_0 \leq 0$  and  $t_1 \geq 1$ . Then

$$\rho_{\text{HG}}(p, q) = \left| \log \frac{(1-t_0)t_1}{(-t_0)(t_1-1)} \right| = \log \left( 1 - \frac{1}{t_0} \right) - \log \left( 1 - \frac{1}{t_1} \right).$$

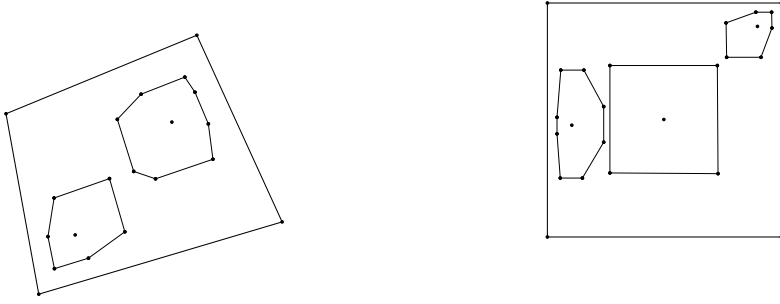


Figure 5: Hilbert balls in quadrangle domains have combinatorial complexity depending on the center location.

The shape of balls in polytope-domain HG is Euclidean polytopes<sup>1</sup> [46], as depicted in Figure 4. Furthermore, the Euclidean shape of the balls does not change with the radius. Hilbert balls have hexagons shapes in 2D [63], rhombic dodecahedra shapes in 3D, and are polytopes [46] with  $d(d+1)$  facets in dimension  $d$ . When the polytope domain is not a simplex, the combinatorial complexity of balls depends on the center location [63], see Figure 5. The HG of the probability simplex yields a non-Riemannian geometry, because, at an infinitesimal radius, the balls are polytopes and not ellipsoids (corresponding to squared Mahalanobis distance balls used to visualize metric tensors [44]). The isometries in Hilbert polyhedral geometries are studied in [48]. In Appendix B, we recall that any Hilbert geometry induces a Finslerian structure that becomes Riemannian iff the boundary is an ellipsoid (yielding the hyperbolic Cayley-Klein geometries [73]). Notice that in Hilbert simplex/polytope geometry, the geodesics are not unique (see Figure 2 of [28]).

## 2.4 $L_1$ -norm geometry

The Total Variation (TV) metric distance between two multinomials  $p$  and  $q$  is defined by:

$$\text{TV}(p, q) = \frac{1}{2} \sum_{i=0}^d |\lambda_p^i - \lambda_q^i|.$$

It is a statistical  $f$ -divergence obtained for the generator  $f(u) = \frac{1}{2}|u - 1|$ . The  $L_1$ -norm induced distance  $\rho_{L1}$  (L1) is defined by:

$$\rho_{L1}(p, q) = \|\lambda_p - \lambda_q\|_1 = \sum_{i=0}^d |\lambda_p^i - \lambda_q^i| = 2\text{TV}(p, q).$$

Therefore the distance  $\rho_{L1}$  satisfies information monotonicity (for coarse-grained histograms  $p'$  and  $q'$  of  $\Delta^{D'}$  with  $D' < D$ ):

$$0 \leq \rho_{L1}(p', q') \leq \rho_{L1}(p, q).$$

For trinomials, the  $\rho_{L1}$  distance is given by:

$$\rho_{L1}(p, q) = |\lambda_p^0 - \lambda_q^0| + |\lambda_p^1 - \lambda_q^1| + |\lambda_q^0 - \lambda_p^0 + \lambda_q^1 - \lambda_p^1|.$$

The  $L_1$  distance function is a polytopal distance function described by the dual polytope  $\mathcal{Z}$  of the  $d$ -dimensional cube called the standard (or regular)  $d$ -cross-polytope [27], the orthoplex [69] or the  $d$ -cocube [17]: The cross-polytope  $\mathcal{Z}$  can be obtained as the convex hull of the  $2d$  unit standard base vectors  $\pm e_i$  for  $i \in \{0, \dots, d-1\}$ . The cross-polytope is one of the three regular polytopes in dimension  $d \geq 4$  (with the hypercubes and simplices): It has  $2d$  vertices and  $2^d$  facets. Therefore the  $L_1$  balls on the hyperplane  $H_{\Delta^d}$  supporting the probability simplex is the intersection of a  $(d+1)$ -cross-polytope with  $d$ -dimensional hyperplane  $H_{\Delta^d}$ . Thus the “multinomial ball”  $\text{Ball}_{L1}(p, r)$  of center  $p$  and radius

<sup>1</sup>To contrast with this result, let us mention that infinitesimal small balls in Riemannian geometry have Euclidean ellipsoidal shapes (visualized as Tissot’s indicatrix in cartography).

Table 1: Comparing the geometric modelings of the probability simplex  $\Delta^d$ .

	<b>Riemannian Geometry</b>	<b>Information Rie. Geo.</b>	<b>Non-Rie. Hilbert Geo.</b>
Structure	$(\Delta^d, g, \nabla^{\text{LC}} = \nabla(g))$ Levi-Civita $\nabla^{\text{LC}} = \nabla^{(0)}$	$(\Delta^d, g, \nabla^{(\alpha)}, \nabla^{(-\alpha)})$ dual connections $\nabla^{(\pm\alpha)}$ so that $\frac{\nabla^{(\alpha)} + \nabla^{(-\alpha)}}{2} = \nabla^{(0)}$	$(\Delta^d, \rho)$ connection of $\mathbb{R}^d$
Distance	Rao distance (metric)	$\alpha$ -divergence (non-metric) KL or reverse KL for $\alpha = \pm 1$	Hilbert distance (metric)
Property	invariant to reparameterization	information monotonicity	isometric to a normed space
Calculation	closed-form	closed-form	easy (Alg. 1)
Geodesic	shortest path	straight either in $\theta/\eta$	straight
Smoothness	manifold	manifold	non-manifold
Curvature	positive	dually flat	negative

$r$  is defined by  $\text{Ball}_{L_1}(p, r) = (\lambda_p \oplus r\mathcal{L}) \cap H_{\Delta^d}$ . In 2D, the shape of  $L_1$  trinomial balls is that of a regular octahedron (twelve edges and eight faces) cut by the 2D plane  $H_{\Delta^2}$ : Trinomial balls have hexagonal shapes as illustrated in Figure 2 (for  $\rho_{L1}$ ). In 3D, trinomial balls are Archimedean solid cuboctahedra, and in arbitrary dimension, the shapes are polytopes with  $d(d+1)$  vertices [13]. Let us note in passing, that in 3D, the  $L_1$  multinomial cuboctahedron ball has the dual shape of the Hilbert rhombic dodecahedron ball.

Table 1 summarizes the characteristics of the three main geometries: FHR, IG, and HG. Let us conclude this introduction by mentioning the Cramér-Rao lower bound and its relationship with information geometry [53]: Consider an unbiased estimator  $\hat{\theta} = T(X)$  of a parameter  $\theta$  estimated from measurements distributed according to a smooth density  $p(x; \theta)$  (i.e.,  $X \sim p(x; \theta)$ ). The Cramér-Rao Lower Bound (CRLB) states that the variance of  $T(X)$  is greater or equal to the inverse of the FIM  $\mathcal{I}(\theta)$ :  $V_\theta[T(X)] \succ \mathcal{I}^{-1}(\theta)$ . For regular parametric families  $\{p(x; \theta)\}_\theta$ , the FIM is a positive-definite matrix and defines a metric tensor, called the Fisher metric in Riemannian geometry. The FIM is the cornerstone of information geometry [4] but requires the differentiability of the probability density function (pdf).

A better lower bound that does not require the pdf differentiability is the Hammersley-Chapman-Robbins Lower Bound [35, 25] (HCRLB):

$$V_\theta[T(X)] \geq \sup_{\Delta} \frac{\Delta^2}{E_\theta \left[ \left( \frac{p(x; \theta + \Delta) - p(x; \theta)}{p(x; \theta)} \right)^2 \right]}. \quad (5)$$

By introducing the  $\chi^2$ -divergence,  $\chi^2(P : Q) = \int \left( \frac{dP - dQ}{dQ} \right)^2 dQ$ , we rewrite the HCRLB using the  $\chi^2$ -divergence in the denominator as follows:

$$V_\theta[T(X)] \geq \sup_{\Delta} \frac{\Delta^2}{\chi^2(P(x; \theta + \Delta) : P(x; \theta))}. \quad (6)$$

Note that the FIM is not defined for non-differentiable pdfs, and therefore the Cramér-Rao lower bound does not exist in that case.

### 3 Computing Hilbert distance in $\Delta^d$

Let us start with the simplest case: The 1D probability simplex  $\Delta^1$ , the space of Bernoulli distributions. Any Bernoulli distribution can be represented by the activation probability of the random bit  $x$ :  $\lambda = p(x=1) \in \Delta^1$ , corresponding to a point in the interval  $\Delta^1 = (0, 1)$ . We write the Bernoulli manifold as an exponential family as

$$p(x) = \exp(x\theta - F(\theta)), \quad x \in \{0, 1\},$$

where  $F(\theta) = \log(1 + \exp(\theta))$ . Therefore  $\lambda = \frac{\exp(\theta)}{1 + \exp(\theta)}$  and  $\theta = \log \frac{\lambda}{1 - \lambda}$ .

### 3.1 1D probability simplex of Bernoulli distributions

By definition, the Hilbert distance has the closed form:

$$\rho_{\text{HG}}(p, q) = \left| \log \frac{\lambda_q(1 - \lambda_p)}{\lambda_p(1 - \lambda_q)} \right| = \left| \log \frac{\lambda_p}{1 - \lambda_p} - \log \frac{\lambda_q}{1 - \lambda_q} \right|.$$

Note that  $\theta_p = \log \frac{\lambda_p}{1 - \lambda_p}$  is the canonical parameter of the Bernoulli distribution.

The FIM of the Bernoulli manifold in the  $\lambda$ -coordinates is given by:  $g = \frac{1}{\lambda} + \frac{1}{1-\lambda} = \frac{1}{\lambda(1-\lambda)}$ . The FHR distance is obtained by integration as:

$$\rho_{\text{FHR}}(p, q) = 2 \arccos \left( \sqrt{\lambda_p \lambda_q} + \sqrt{(1 - \lambda_p)(1 - \lambda_q)} \right).$$

Notice that  $\rho_{\text{FHR}}(p, q)$  has finite values on  $\partial\Delta^1$ .

The KL divergence of the  $\pm 1$ -geometry is:

$$\rho_{\text{IG}}(p, q) = \lambda_p \log \frac{\lambda_p}{\lambda_q} + (1 - \lambda_p) \log \frac{1 - \lambda_p}{1 - \lambda_q}.$$

The KL divergence belongs to the family of  $\alpha$ -divergences [4].

### 3.2 Arbitrary dimension case

Given  $p, q \in \Delta^d$ , we first need to compute the intersection of line  $(pq)$  with the border of the  $d$ -dimensional probability simplex to get the two intersection points  $p'$  and  $q'$  so that  $p', p, q, q'$  are ordered on  $(pq)$ . Once this is done, we simply apply the formula in Eq. 4 to get the Hilbert distance.

A  $d$ -dimensional simplex consists of  $d + 1$  vertices with their corresponding  $(d - 1)$ -dimensional facets. For the probability simplex  $\Delta^d$ , let  $e_i = (\underbrace{0, \dots, 0}_i, 1, 0, \dots, 0)$  denote the  $d + 1$  vertices of the standard simplex embedded in the

hyperplane  $H_\Delta : \sum_{i=0}^d \lambda^i = 1$  in  $\mathbb{R}^{d+1}$ . Let  $f_{\setminus j}$  denote the simplex facets that is the convex hull of all vertices except  $e_j$ :  $f_{\setminus j} = \text{hull}(e_0, \dots, e_{j-1}, e_{j+1}, \dots, e_d)$ . Let  $H_{\setminus j}$  denote the hyperplane supporting this facet, which is the affine hull  $f_{\setminus j} = \text{affine}(e_0, \dots, e_{j-1}, e_{j+1}, \dots, e_d)$ .

To compute the two intersection points of  $(pq)$  with  $\Delta^d$ , a naive algorithm consists in computing the unique intersection point  $r_j$  of the line  $(pq)$  with each hyperplane  $H_{\setminus j}$  ( $j = 0, \dots, d$ ) and checking whether  $r_j$  belongs to  $f_{\setminus j}$ .

A much more efficient implementation given by Alg. (1) calculates the intersection point of the line  $x(t) = (1 - t)p + tq$  with each  $H_{\setminus j}$  ( $j = 0, \dots, d$ ). These intersection points are represented using the coordinate  $t$ . For example,  $x(0) = p$  and  $x(1) = q$ . Due to convexity, any intersection point with  $H_{\setminus j}$  must satisfy either  $t \leq 0$  or  $t \geq 1$ . Then, the two intersection points with  $\partial\Delta^d$  are obtained by  $t_0 = \max\{t : \exists j, x(t) \in H_{\setminus j} \text{ and } t \leq 0\}$  and  $t_1 = \min\{t : \exists j, x(t) \in H_{\setminus j} \text{ and } t \geq 1\}$ . Figure 6 illustrates this calculation method. This algorithm only requires  $O(d)$  time and  $O(1)$  memory.

**Lemma 1.** *The Hilbert distance in the probability simplex can be computed in optimal  $\Theta(d)$  time.*

Once an arbitrary distance  $\rho$  is chosen, we can define a ball centered at  $c$  and of radius  $r$  as  $B_\rho(c, r) = \{x : \rho(c, x) \leq r\}$ . Figure 4 displays the hexagonal shapes of the Hilbert balls for various center locations in  $\Delta^2$ .

**Theorem 1** (Balls in a simplicial Hilbert geometry [46]). *A ball in the Hilbert simplex geometry has a Euclidean polytope shape with  $d(d + 1)$  facets.*

Note that when the domain is not simplicial, the Hilbert balls can have varying combinatorial complexity depending on the center location. In 2D, the Hilbert ball can have  $s \sim 2s$  edges inclusively, where  $s$  is the number of edges of the boundary of the Hilbert domain  $\partial\mathcal{C}$ .

Since a Riemannian geometry is locally defined by a metric tensor, at infinitesimal scales, Riemannian balls have Mahalanobis smooth ellipsoidal shapes:  $B_\rho(c, r) = \{x : (x - c)^\top g(c)(x - c) \leq r^2\}$ . This property allows one to visualize Riemannian metric tensors [44]. Thus we conclude that:

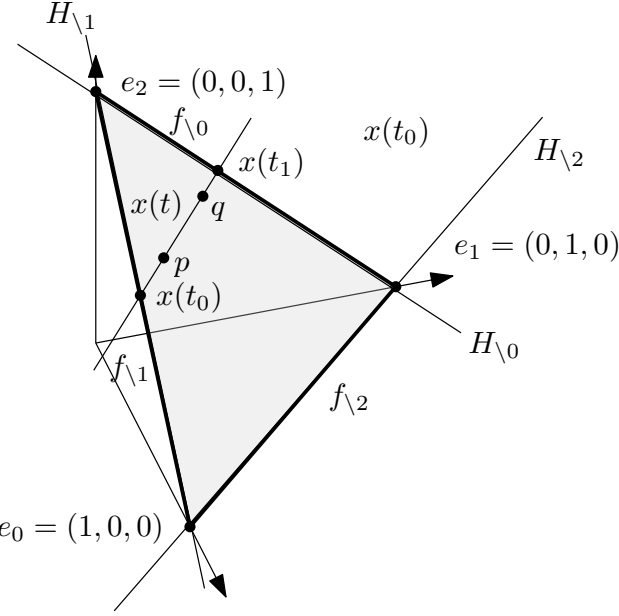


Figure 6: Calculating the two intersection points  $x(t_0)$  and  $x(t_1)$  of the line  $(pq)$  with the boundary of the probability simplex  $\Delta_d$ : For each facet  $f_{\backslash i}$ , we calculate the intersection point of line  $x(t) = (1-t)p + tq$  with the  $d$ -dimensional hyperplane  $H_{\backslash i}$  supporting the facet  $f_{\backslash i}$ .

**Lemma 2** ([46]). *Hilbert simplex geometry is a non-manifold metric length space.*

As a remark, let us notice that slicing a simplex with a hyperplane does not always produce a lower-dimensional simplex. For example, slicing a tetrahedron by a plane yields either a triangle or a quadrilateral. Thus the restriction of a  $d$ -dimensional ball  $B$  in a Hilbert simplex geometry  $\Delta^d$  to a hyperplane  $H$  is a  $(d-1)$ -dimensional ball  $B' = B \cap H$  of varying combinatorial complexity, corresponding to a ball in the induced Hilbert sub-geometry in the convex sub-domain  $H \cap \Delta^d$ .

### 3.3 Hilbert simplex distance satisfies the information monotonicity

Let us prove that the Hilbert simplex metric satisfies the property of information monotonicity.

Instead of considering the Hilbert simplex metric on the  $(d-1)$ -dimensional simplex  $\Delta_d$ , we consider the equivalent Hilbert simplex *projective* metric  $\rho_{BG}$  defined on the cone  $\mathbb{R}_{+,*}^d$ . We call  $\rho_{BG}$  the *Birkhoff metric* [16] since it measures the distance between any two cone rays, say  $\tilde{p}$  and  $\tilde{q}$  of  $\mathbb{R}_{+,*}^d$ . The Birkhoff metric [16] is defined by:

$$\rho_{BG}(\tilde{p}, \tilde{q}) := \log \max_{i,j} \frac{\tilde{p}_i \tilde{q}_j}{\tilde{p}_j \tilde{q}_i}, \quad (7)$$

and is scale-invariant:

$$\rho_{BG}(\alpha \tilde{p}, \alpha \tilde{q}) = \rho_{BG}(\tilde{p}, \tilde{q}), \quad (8)$$

for any  $\alpha, \beta > 0$ . We have  $\rho_{BG}(\tilde{p}, \tilde{q}) = 0$  if and only if  $\tilde{p} = \lambda \tilde{q}$  for  $\lambda > 0$ . Thus we define *equivalence classes*  $\tilde{p} \sim \tilde{q}$  when there exists  $\lambda > 0$  such that  $\tilde{p} = \lambda \tilde{q}$ . The Birkhoff metric satisfies the triangle inequality and is therefore a *projective metric* [21]. For a ray  $\tilde{r}$  in  $\mathbb{R}_{+,*}^d$ , let  $r$  denote the intersection of  $\tilde{r}$  with the standard simplex  $\Delta_d$ . Inhomogeneous vector  $r \in \Delta_d$  is obtained by dehomogenizing the ray vector so that  $\sum_{i=1}^d r_i = 1$ . For a ray  $\tilde{r}$ , let  $\tilde{r} = r$  denote the dehomogenization. Then we have:

$$\rho_{BG}(\tilde{p}, \tilde{q}) = \rho_{HG}(p, q). \quad (9)$$

---

**Algorithm 1:** Computing the Hilbert distance

---

**Data:** Two points  $p = (\lambda_p^0, \dots, \lambda_p^d)$ ,  $q = (\lambda_q^0, \dots, \lambda_q^d)$  in the  $d$ -dimensional simplex  $\Delta^d$

**Result:** Their Hilbert distance  $\rho_{\text{HG}}(p, q)$

```

1 begin
2    $t_0 \leftarrow -\infty; t_1 \leftarrow +\infty;$ 
3   for  $i = 0 \dots d$  do
4     if  $\lambda_p^i \neq \lambda_q^i$  then
5        $t \leftarrow \lambda_p^i / (\lambda_p^i - \lambda_q^i);$ 
6       if  $t_0 < t \leq 0$  then
7          $t_0 \leftarrow t;$ 
8       else if  $1 \leq t < t_1$  then
9          $t_1 \leftarrow t;$ 
10
11  if  $t_0 = -\infty$  or  $t_1 = +\infty$  then
12    Output  $\rho_{\text{HG}}(p, q) = 0;$ 
13  else if  $t_0 = 0$  or  $t_1 = 1$  then
14    Output  $\rho_{\text{HG}}(p, q) = \infty;$ 
15  else
16    Output  $\rho_{\text{HG}}(p, q) = \left| \log\left(1 - \frac{1}{t_0}\right) - \log\left(1 - \frac{1}{t_1}\right) \right|;$ 

```

---

The Birkhoff metric can be calculated using an equivalent norm-induced distance on the logarithmic representation:

$$\rho_{\text{BG}}(\tilde{p}, \tilde{q}) = \|\log(\tilde{p}) - \log(\tilde{q})\|_{\text{var}}, \quad (10)$$

where  $\|x\|_{\text{var}} := (\max_i x_i) - (\min_i x_i)$  is the *variation norm*, and  $\log(x) = (\log x_1, \dots, \log x_d)$ . Notice that computing  $\rho_{\text{BG}}(p, q) = \|\log(p) - \log(q)\|_{\text{var}}$  yields a simple linear-time algorithm to compute the Hilbert simplex distance.

Figure 7 illustrates the relationship between the Hilbert simplex metric and the Birkhoff projective cone metric.

Now, consider a bounded linear positive operator  $M : \mathbb{R}_+^d \rightarrow \mathbb{R}_+^{d'}$  with  $d' < d$  and  $M_{ij} > 0$  which encodes the coarse-binning scheme of the standard simplex  $\Delta_d$  into the standard simplex  $\Delta_{d'}$ . A  $d$ -dimensional positive measure  $\tilde{r}$  is mapped into a  $d'$ -dimensional positive measure  $\tilde{p}'$  such that  $\tilde{p}' = M\tilde{r}$ . Matrix  $M$  is a  $d' \times d$  (fat) positive matrix that is column-stochastic (i.e., elements of each column sum up to one).

Birkhoff proved [16] (1957) that:

$$\rho_{\text{BG}}(M\tilde{p}, M\tilde{q}) \leq \kappa(M)\rho_{\text{BG}}(\tilde{p}, \tilde{q}), \quad (11)$$

where  $\kappa(M)$  is the *contraction ratio* of the binning scheme. Furthermore, it can be shown that:

$$\kappa(M) := \frac{\sqrt{a(M)} - 1}{\sqrt{a(M)} + 1} < 1, \quad (12)$$

with

$$a(M) := \max_{i,j,k,l} \frac{M_{i,k}M_{j,l}}{M_{j,k}M_{i,l}} < \infty. \quad (13)$$

Thus coarse-binning the probability simplex  $\Delta_d$  to  $\Delta_{d'}$  makes a *strict contraction* of the distance between distinct elements.

**Theorem 2.** *The Hilbert simplex metric is a non-separable distance satisfying the property of information monotonicity.*

Notice that this proof<sup>2</sup> is based on a contraction theorem of a bounded linear positive operator, and that therefore the information monotonicity property may be rewritten equivalently as a contraction property.

<sup>2</sup>Birkhoff's proof [16] is more general and works for any projective distance defined over a cone (so-called Hilbert projective distances) by defining the notion of projective diameter of a positive linear operator.

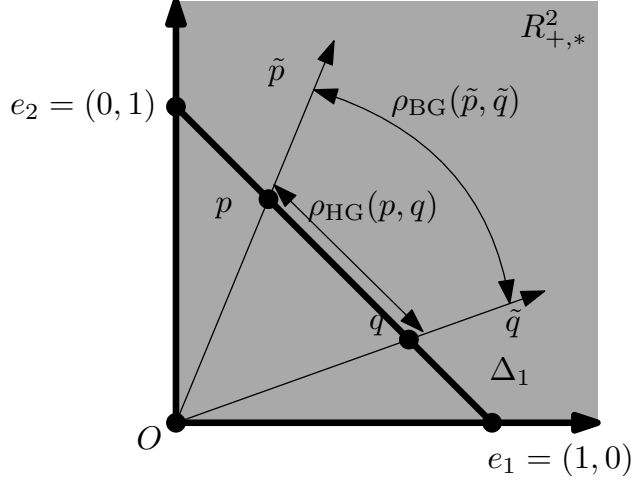


Figure 7: Illustration of the equivalence between the Hilbert simplex metric  $\rho_{\text{HG}}$  and the Birkhoff projective metric  $\rho_{\text{BG}}$  defined over the positive orthant.

In information geometry, it is known that the class of separable divergences satisfying the information monotonicity are  $f$ -divergences when  $d > 2$ , see [4] (see [40] for the special case  $d = 2$  corresponding to binary alphabets). It is an open problem to fully characterize the class of *non-separable distances* that fulfills the property of information monotonicity.

### 3.4 Visualizing distance profiles

Figure 8 displays the distance profile from any point in the probability simplex to a fixed reference point (trinomial) based on the following common distance measures [22]: Euclidean (metric) distance, Cauchy-Schwarz (CS) divergence, Hellinger (metric) distance, Fisher-Rao (metric) distance, KL divergence and Hilbert simplicial (metric) distance. The Euclidean and Cauchy-Schwarz divergence are clipped to  $\Delta^2$ . The Cauchy-Schwarz distance is projective so that  $\rho_{\text{CS}}(\lambda p, \lambda' q) = \rho_{\text{CS}}(p, q)$  for any  $\lambda, \lambda' > 0$  [65].

## 4 Center-based clustering

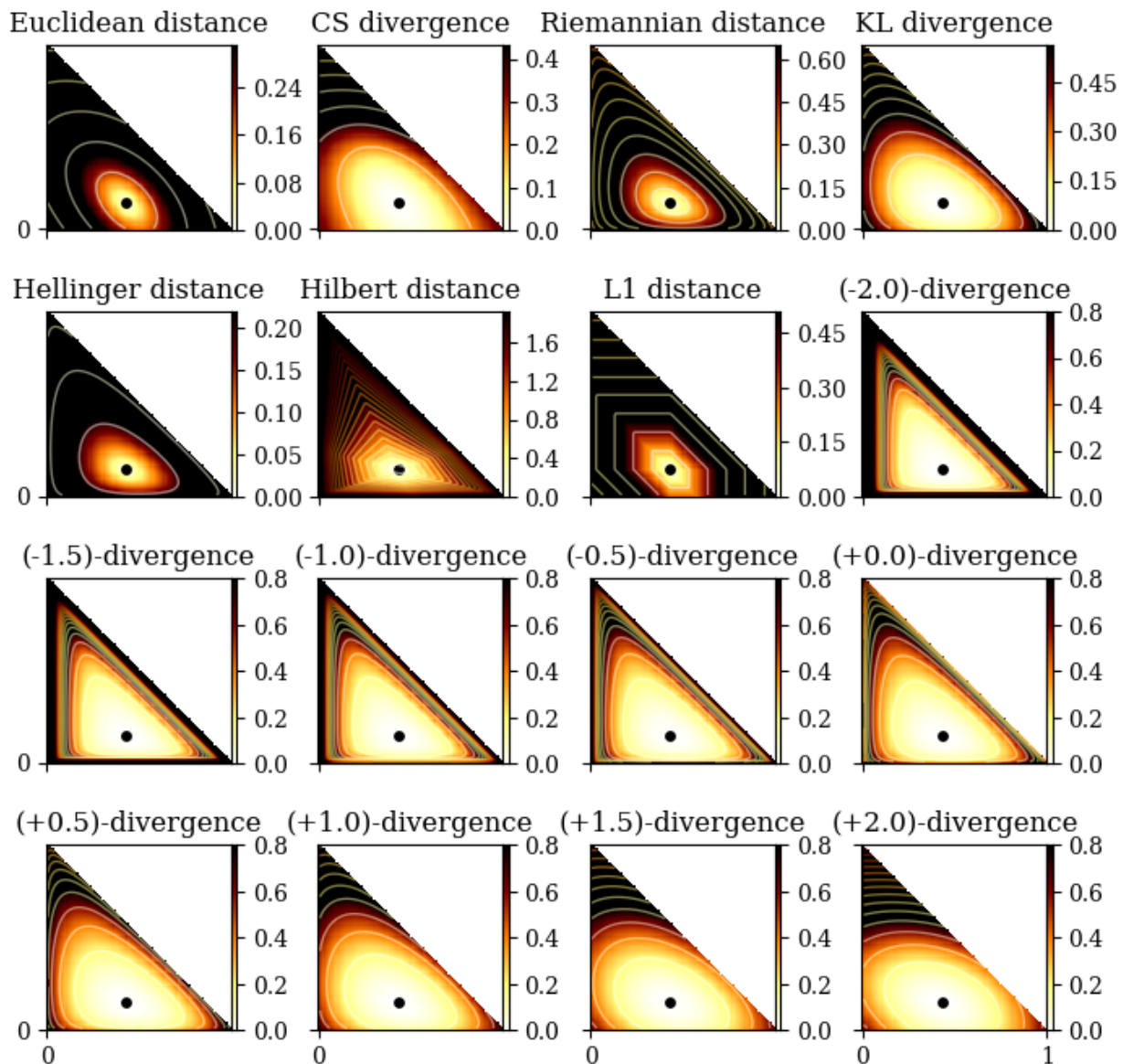
We concentrate on comparing the efficiency of Hilbert simplex geometry for clustering multinomials. We shall compare the experimental results of  $k$ -means++ and  $k$ -center multinomial clustering for the three distances: Rao and Hilbert metric distances, and KL divergence. We describe how to adapt those clustering algorithms to the Hilbert distance.

### 4.1 $k$ -means++ clustering

The celebrated  $k$ -means clustering [61] minimizes the sum of within-cluster variances, where each cluster has a center representative element. When dealing with  $k = 1$  cluster, the center (also called centroid or cluster prototype) is the center of mass defined as the minimizer of

$$E_D(\Lambda, c) = \frac{1}{n} \sum_{i=1}^n D(p_i : c),$$

where  $D(\cdot : \cdot)$  is a dissimilarity measure. For an arbitrary  $D$ , the centroid  $c$  may not be available in closed form. Nevertheless, using a generalization of the  $k$ -means++ initialization [8] (picking randomly seeds), one can bypass the centroid computation, and yet guarantee probabilistically a good clustering.



(a) Reference point  $(\frac{3}{7}, \frac{3}{7}, \frac{1}{7})$

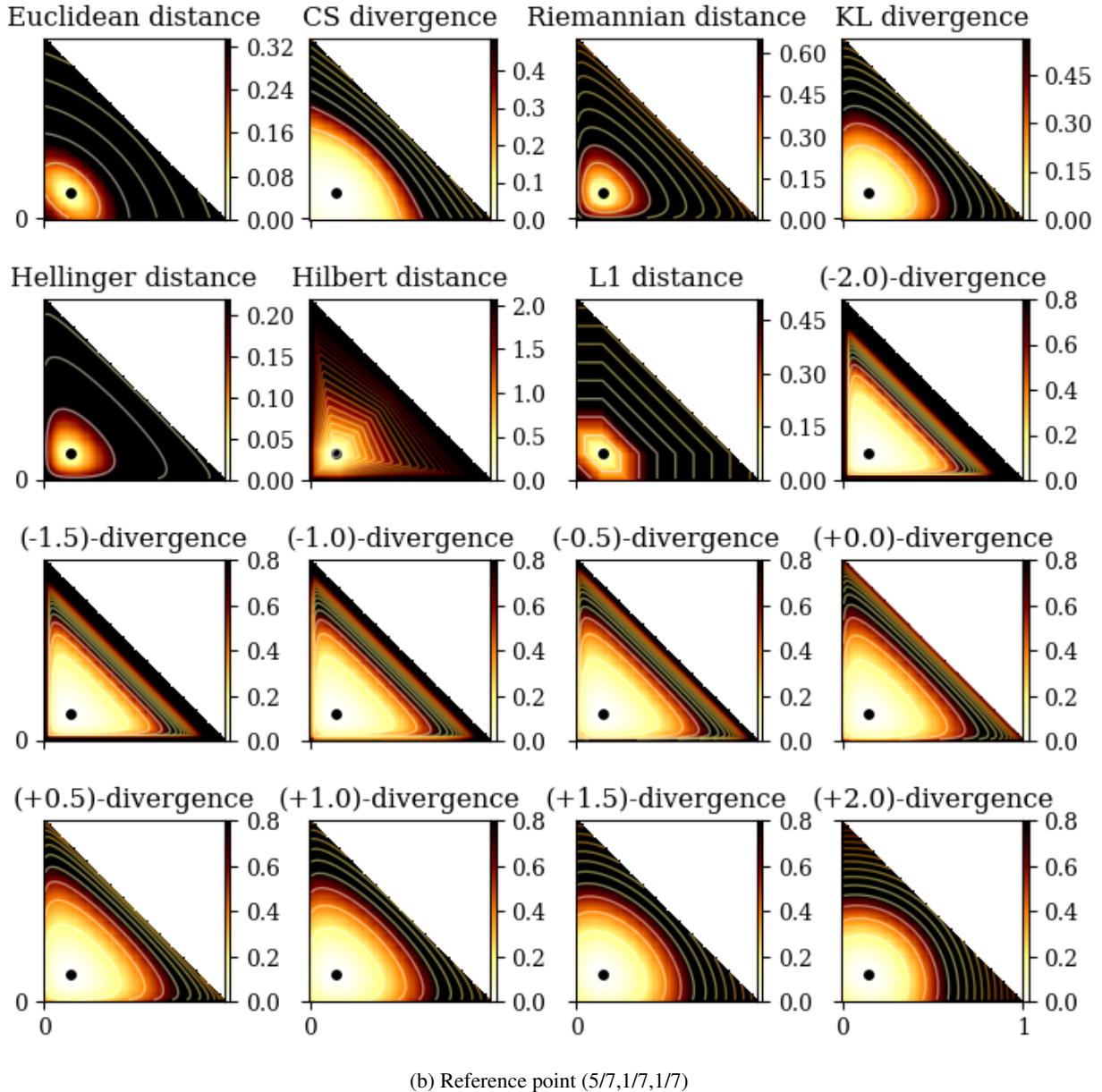


Figure 8: A comparison of different distance measures on  $\Delta^2$ . The distance is measured from  $\forall p \in \Delta^2$  to a fixed reference point (the black dot). Lighter color means shorter distance. Darker color means longer distance. The contours show equal distance curves with a precision step of 0.2.

Let  $C = \{c_1, \dots, c_k\}$  denote the set of  $k$  cluster centers. Then the generalized  $k$ -means energy to be minimized is defined by:

$$E_D(\Lambda, C) = \frac{1}{n} \sum_{i=1}^n \min_{j \in \{1, \dots, k\}} D(p_i : c_j).$$

By defining the distance  $D(p, C) = \min_{j \in \{1, \dots, k\}} D(p : c_j)$  of a point to a set, we can rewrite the objective function as  $E_D(\Lambda, C) = \frac{1}{n} \sum_{i=1}^n D(p_i, C)$ . Let  $E_D^*(\Lambda, k) = \min_{C : |C|=k} E_D(\Lambda, C)$  denote the global minimum of  $E_D(\Lambda, C)$  wrt some given  $\Lambda$  and  $k$ .

The  $k$ -means++ seeding proceeds for an arbitrary divergence  $D$  as follows: Pick uniformly at random at first seed  $c_1$ , and then iteratively choose the  $(k - 1)$  remaining seeds according to the following probability distribution:

$$\Pr(c_j = p_i) = \frac{D(p_i, \{c_1, \dots, c_{j-1}\})}{\sum_{i=1}^n D(p_i, \{c_1, \dots, c_{j-1}\})} \quad (2 \leq j \leq k).$$

Since its inception (2007), this  $k$ -means++ seeding has been extensively studied [9]. We state the general theorem established by [60]:

**Theorem 3** (Generalized  $k$ -means++ performance, [60]). *Let  $\kappa_1$  and  $\kappa_2$  be two constants such that  $\kappa_1$  defines the quasi-triangular inequality property:*

$$D(x : z) \leq \kappa_1 (D(x : y) + D(y : z)), \quad \forall x, y, z \in \Delta^d,$$

and  $\kappa_2$  handles the symmetry inequality:

$$D(x : y) \leq \kappa_2 D(y : x), \quad \forall x, y \in \Delta^d.$$

Then the generalized  $k$ -means++ seeding guarantees with high probability a configuration  $C$  of cluster centers such that:

$$E_D(\Lambda, C) \leq 2\kappa_1^2 (1 + \kappa_2) (2 + \log k) E_D^*(\Lambda, k). \quad (14)$$

The ratio  $\frac{E_D(\Lambda, C)}{E_D^*(\Lambda, k)}$  is called the *competitive factor*. The seminal result of ordinary  $k$ -means++ was shown [8] to be  $8(2 + \log k)$ -competitive. When evaluating  $\kappa_1$ , one has to note that squared metric distances are not metric because they do not satisfy the triangular inequality. For example, the squared Euclidean distance is not a metric but it satisfies the 2-quasi-triangular inequality with  $\kappa_1 = 2$ .

We state the following general performance theorem:

**Theorem 4** ( $k$ -means++ performance in a metric space). *In any metric space  $(\mathcal{X}, d)$ , the  $k$ -means++ wrt the squared metric distance  $d^2$  is  $16(2 + \log k)$ -competitive.*

*Proof.* Since a metric distance is symmetric, it follows that  $\kappa_2 = 1$ . Consider the quasi-triangular inequality property for the squared non-metric dissimilarity  $d^2$ :

$$\begin{aligned} d(p, q) &\leq d(p, q) + d(q, r), \\ d^2(p, q) &\leq (d(p, q) + d(q, r))^2, \\ d^2(p, q) &\leq d^2(p, q) + d^2(q, r) + 2d(p, q)d(q, r). \end{aligned}$$

Let us apply the inequality of arithmetic and geometric means<sup>3</sup>:

$$\sqrt{d^2(p, q)d^2(q, r)} \leq \frac{d^2(p, q) + d^2(q, r)}{2}.$$

Thus we have

$$d^2(p, q) \leq d^2(p, q) + d^2(q, r) + 2d(p, q)d(q, r) \leq 2(d^2(p, q) + d^2(q, r)).$$

That is, the squared metric distance satisfies the 2-approximate triangle inequality, and  $\kappa_1 = 2$ . The result is straightforward from Theorem 3.  $\square$

---

<sup>3</sup>For positive values  $a$  and  $b$ , the arithmetic-geometric mean inequality states that  $\sqrt{ab} \leq \frac{a+b}{2}$ .

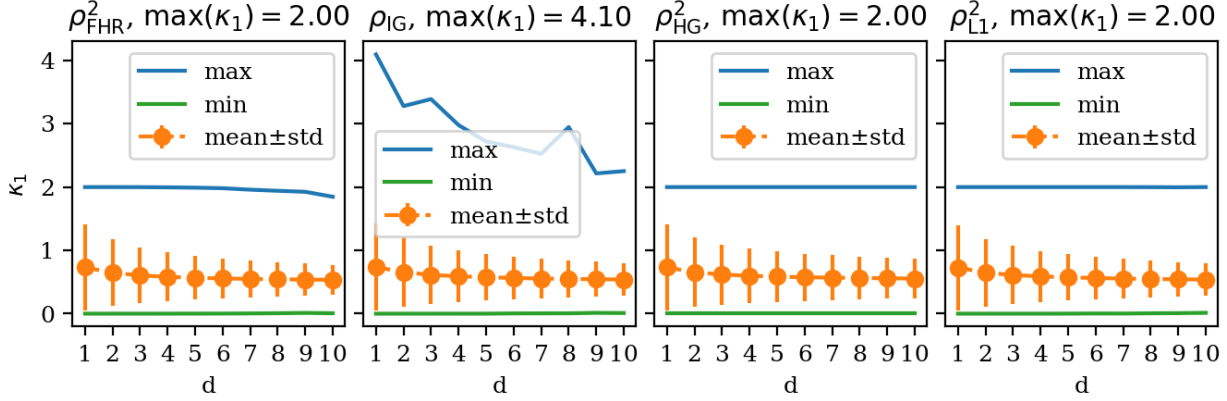


Figure 9: The maximum, mean, standard deviation, and minimum of  $\kappa_1$  on  $10^6$  randomly generated tuples  $(x, y, z)$  in  $\Delta^d$  for  $d = 1, \dots, 10$ .

**Theorem 5** ( $k$ -means++ performance in a normed space). *In any normed space  $(\mathcal{X}, \|\cdot\|)$ , the  $k$ -means++ with  $D(x:y) = \|x-y\|^2$  is  $16(2 + \log k)$ -competitive.*

*Proof.* In any normed space  $(\mathcal{X}, \|\cdot\|)$ , we have both  $\|x-y\| = \|y-x\|$  and the triangle inequality:

$$\|x-z\| \leq \|x-y\| + \|y-z\|.$$

The proof is very similar to the proof of Theorem 4 and is omitted.  $\square$

Since any inner product space  $(\mathcal{X}, \langle \cdot, \cdot \rangle)$  has an induced norm  $\|x\| = \sqrt{\langle x, x \rangle}$ , we have the following corollary.

**Corollary 1.** *In any inner product space  $(\mathcal{X}, \langle \cdot, \cdot \rangle)$ , the  $k$ -means++ with  $D(x:y) = \langle x-y, x-y \rangle$  is  $16(2 + \log k)$ -competitive.*

We need to report a bound for the squared Hilbert symmetric distance ( $\kappa_2 = 1$ ). In [46] (Theorem 3.3), it was shown that Hilbert geometry of a bounded convex domain  $\mathcal{C}$  is isometric to a normed vector space iff  $\mathcal{C}$  is an open simplex:  $(\Delta^d, \rho_{\text{HG}}) \simeq (V^d, \|\cdot\|_{\text{NH}})$ , where  $\|\cdot\|_{\text{NH}}$  is the corresponding norm. Therefore  $\kappa_1 = 2$ . We write “NH” for short for this equivalent normed Hilbert geometry. Appendix A recalls the construction due to [28], and shows the squared Hilbert distance fails the triangle inequality and it is not a distance induced by an inner product.

As an empirical study, we randomly generate  $n = 10^6$  tuples  $(x, y, z)$  based on the uniform distribution in  $\Delta^d$ . For each tuple  $(x, y, z)$ , we evaluate the ratio

$$\kappa_1 = \frac{D(x:z)}{D(x:y) + D(y:z)}.$$

Figure 9 shows the statistics for four different choices of  $D$ : (1)  $D(x:y) = \rho_{\text{FHR}}^2(x,y)$ ; (2)  $D(x:y) = \frac{1}{2}\text{KL}(x:y) + \frac{1}{2}\text{KL}(y:x)$ ; (3)  $D(x:y) = \rho_{\text{HG}}^2(x,y)$ ; (4)  $D(x:y) = \rho_{\text{L1}}^2(x,y)$ . We find experimentally that  $\kappa_1$  is upper bounded by 2 for  $\rho_{\text{FHR}}^2$ ,  $\rho_{\text{HG}}^2$  and  $\rho_{\text{L1}}^2$ , while the average  $\kappa_1$  value is smaller than 0.5. For all the compared distances,  $\kappa_2 = 1$ . Therefore  $\rho_{\text{FHR}}$  and  $\rho_{\text{HG}}$  have better  $k$ -means++ performance guarantee as compared to  $\rho_{\text{IG}}$ .

We get by applying Theorem 5:

**Corollary 2** ( $k$ -means++ in Hilbert simplex geometry). *The  $k$ -means++ seeding in a Hilbert simplex geometry in fixed dimension is  $16(2 + \log k)$ -competitive.*

Figure 10 displays the clustering results of  $k$ -means++ in Hilbert simplex geometry as compared to the other geometries for  $k \in \{3, 5\}$ .

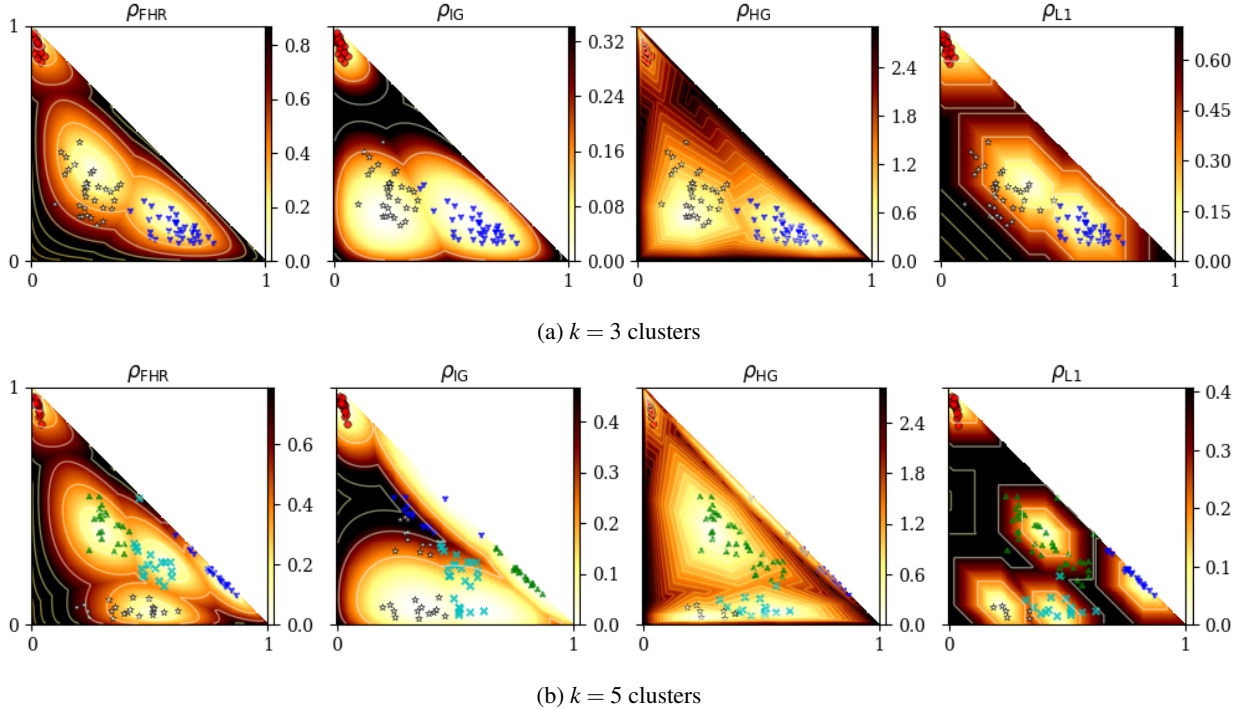


Figure 10:  $k$ -Means++ clustering results on a toy dataset in the space of trinomials  $\Delta^2$ . The color density maps indicate the distance from any point to its nearest cluster center.

The KL divergence can be interpreted as a separable Bregman divergence [1]. The Bregman  $k$ -means++ performance has been studied in [1, 50], and a competitive factor of  $O(\frac{1}{\mu})$  is reported using the notion of Bregman  $\mu$ -similarity (that is suited for data-sets on a compact domain).

In [32], spherical  $k$ -means++ is studied wrt the distance  $d_S(x, y) = 1 - \langle x, y \rangle$  for any pair of points  $x, y$  on the unit sphere. Since  $\langle x, y \rangle = \|x\|_2 \|y\|_2 \cos(\theta_{x,y}) = \cos(\theta_{x,y})$ , we have  $d_S(x, y) = 1 - \cos(\theta_{x,y})$ , where  $\theta_{x,y}$  denotes the angle between a pair of unit vectors  $x$  and  $y$ . This distance is called the cosine distance since it amounts to one minus the cosine similarity. Notice that the cosine distance is related to the squared Euclidean distance via the identity:  $d_S(x, y) = \frac{1}{2} \|x - y\|^2$ . The cosine distance is different from the spherical distance that relies on the arccos function.

Since divergences may be asymmetric, one can further consider mixed divergence  $M(p : q : r) = \lambda D(p : q) + (1 - \lambda)D(q : r)$  for  $\lambda \in [0, 1]$ , and extend the  $k$ -means++ seeding procedure and analysis [62].

For a given data set, we can compute  $\kappa_1$  or  $\kappa_2$  by inspecting triples and pairs of points, and get data-dependent competitive factor improving the bounds mentioned above.

## 4.2 $k$ -Center clustering

Let  $\Lambda$  be a finite point set. The cost function for a  $k$ -center clustering with centers  $C$  ( $|C| = k$ ) is:

$$f_D(\Lambda, C) = \max_{p_i \in \Lambda} \min_{c_j \in C} D(p_i : c_j).$$

The farthest first traversal heuristic [34] has a guaranteed approximation factor of 2 for any metric distance (see Algorithm 3).

In order to use the  $k$ -center clustering algorithm described in Algorithm 2, we need to be able to compute the 1-center (or minimax center) for the Hilbert simplex geometry, that is the Minimum Enclosing Ball (MEB, also called the Smallest Enclosing Ball, SEB).

---

**Algorithm 2:**  $k$ -Center clustering

---

**Data:** A set of points  $p_1, \dots, p_n \in \Delta^d$ . A distance measure  $\rho$  on  $\Delta^d$ . The maximum number  $k$  of clusters. The maximum number  $T$  of iterations.

**Result:** A clustering scheme assigning each  $p_i$  a label  $l_i \in \{1, \dots, k\}$

```

1 begin
2   Randomly pick  $k$  cluster centers  $c_1, \dots, c_k$  using the kmeans++ heuristic;
3   for  $t = 1, \dots, T$  do
4     for  $i = 1, \dots, n$  do
5        $l_i \leftarrow \arg \min_{l=1}^k \rho(p_i, c_l);$ 
6     for  $l = 1, \dots, k$  do
7        $c_l \leftarrow \arg \min_c \max_{i: l_i=l} \rho(p_i, c);$ 
8   Output  $\{l_i\}_{i=1}^n;$ 

```

---

**Algorithm 3:** A 2-approximation of the  $k$ -center clustering for any metric distance  $\rho$ .

---

**Data:** A set  $\Lambda$ ; a number  $k$  of clusters; a metric distance  $\rho$ .

**Result:** A 2-approximation of the  $k$ -center clustering

```

1 begin
2    $c_1 \leftarrow \text{ARandomPointOf}(\Lambda);$ 
3    $C \leftarrow \{c_1\};$ 
4   for  $i = 2, \dots, k$  do
5      $c_i \leftarrow \arg \max_{p \in \Lambda} \rho(p, C);$ 
6      $C \leftarrow C \cup \{c_i\};$ 
7 Output  $C;$ 

```

---

We may consider the SEB equivalently either in  $\Delta^d$  or in the normed space  $V^d$ . In both spaces, the shapes of the balls are convex. Let  $\Lambda = \{p_1, \dots, p_n\}$  denote the point set in  $\Delta^d$ , and  $\mathcal{V} = \{v_1, \dots, v_n\}$  the equivalent point set in the normed vector space (following the mapping explained in Appendix A). Then the SEBs  $B_{\text{HG}}(\Lambda)$  in  $\Delta^d$  and  $B_{\text{NH}}(\mathcal{V})$  in  $V^d$  have respectively radii  $r_{\text{HG}}^*$  and  $r_{\text{NH}}^*$  defined by:

$$\begin{aligned} r_{\text{HG}}^* &= \min_{c \in \Delta^d} \max_{i \in \{1, \dots, n\}} \rho_{\text{HG}}(p_i, c), \\ r_{\text{NH}}^* &= \min_{v \in V^d} \max_{i \in \{1, \dots, n\}} \|v_i - v\|_{\text{NH}}. \end{aligned}$$

The SEB in the normed vector space  $(V^d, \|\cdot\|_{\text{NH}})$  amounts to find the minimum covering norm polytope of a finite point set. This problem has been well-studied in computational geometry [75, 18, 67]. By considering the equivalent Hilbert norm polytope with  $d(d+1)$  facets, we state the result of [75]:

**Theorem 6** (SEB in Hilbert polytope normed space, [75]). *A  $(1 + \epsilon)$ -approximation of the SEB in  $V^d$  can be computed in  $O(d^3 \frac{n}{\epsilon})$  time.*

We shall now report two algorithms for computing the SEBs: One exact algorithm in  $V^d$  that does not scale well in high dimensions, and one approximation in  $\Delta^d$  that works well for large dimensions.

#### 4.2.1 Exact smallest enclosing ball in a Hilbert simplex geometry

Given a finite point set  $\{p_1, \dots, p_n\} \in \Delta^d$ , the SEB in Hilbert simplex geometry is centered at

$$c^* = \arg \min_{c \in \Delta^d} \max_{i \in \{1, \dots, n\}} \rho_{\text{HG}}(c, x_i),$$

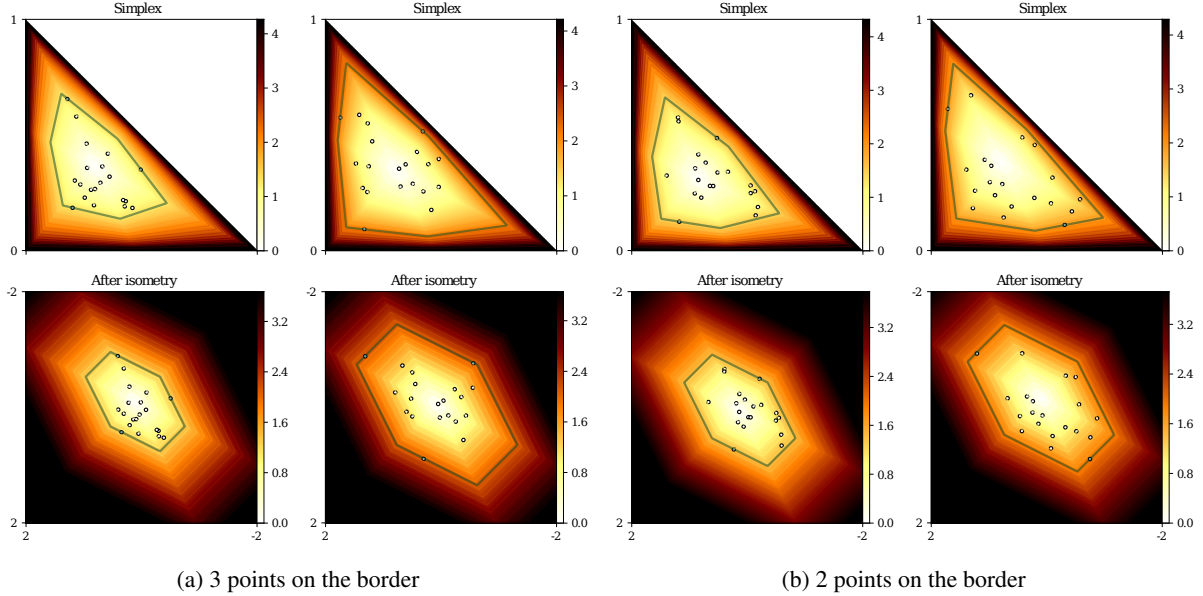


Figure 11: Computing the SEB in Hilbert simplex geometry amounts to compute the SEB in the corresponding normed vector space.

with radius

$$r^* = \min_{c \in \Delta^d} \max_{i \in \{1, \dots, n\}} \rho_{\text{HG}}(c, x_i).$$

An equivalent problem is to find the SEB in the isometric normed vector space  $V^d$  via the mapping reported in Appendix A. Each simplex point  $p_i$  corresponds to a point  $v_i$  in the  $V^d$ .

Figure 11 displays some examples of the exact smallest enclosing balls in the Hilbert simplex geometry and in the corresponding normed vector space.

To compute the SEB, one may also consider the generic LP-type randomized algorithm [58]. We notice that an enclosing ball for a point set in general has a number  $k$  of points on the border of the ball, with  $2 \leq k \leq \frac{d(d+1)}{2}$ . Let  $D = \frac{d(d+1)}{2}$  denote the varying size of the combinatorial basis, then we can apply the LP-type framework (we check the axioms of locality and monotonicity, [76]) to solve efficiently the SEBs.

**Theorem 7** (Smallest Enclosing Hilbert Ball is LP-type, [83, 76]). *The smallest enclosing Hilbert ball amounts to find the smallest enclosing ball in a vector space with respect to a polytope norm that can be solved using a LP-type randomized algorithm.*

The Enclosing Ball Decision Problem (EBDP, [59]) asks for a given value  $r$ , whether  $r \geq r^*$  or not. The decision problem amounts to find whether a set  $\{rB_V + v_i\}$  of translates can be stabbed by a point [59]: That is, whether  $\cap_{i=1}^n (rB_V + v_i)$  is empty or not. Since these translates are polytopes with  $d(d+1)$  facets, this can be solved in linear time using *Linear Programming*.

**Theorem 8** (Enclosing Hilbert Ball Decision Problem). *The decision problem to test whether  $r \geq r^*$  or not can be solved by Linear Programming.*

This yields a simple scheme to approximate the optimal value  $r^*$ : Let  $r_0 = \max_{i \in \{2, \dots, n\}} \|v_i - v_1\|_{\text{NH}}$ . Then  $r^* \in [\frac{r_0}{2}, r_0] = [a_0, b_0]$ . At stage  $i$ , perform a dichotomic search on  $[a_i, b_i]$  by answering the decision problem for  $r_{i+1} = \frac{a_i+b_i}{2}$ , and update the radius range accordingly [59].

However, the LP-type randomized algorithm or the decision problem-based algorithm do not scale well in high dimensions. Next, we introduce a simple approximation algorithm that relies on the fact that the line segment  $[pq]$  is a geodesic in Hilbert simplex geometry. (Geodesics are not unique. See Figure 2 of [28].)

#### 4.2.2 Geodesic bisection approximation heuristic

In Riemannian geometry, the 1-center can be arbitrarily finely approximated by a simple geodesic bisection algorithm [11, 7]. This algorithm can be extended to HG straightforwardly as detailed in Algorithm 4.

---

**Algorithm 4:** Geodesic walk for approximating the Hilbert minimax center, generalizing [11]

---

**Data:** A set of points  $p_1, \dots, p_n \in \Delta^d$ . The maximum number  $T$  of iterations.

**Result:**  $c \approx \arg \min_c \max_i \rho_{\text{HG}}(p_i, c)$

```

1 begin
2    $c_0 \leftarrow \text{ARandomPointOf}(\{p_1, \dots, p_n\})$ ;
3   for  $t = 1, \dots, T$  do
4      $p \leftarrow \arg \max_{p_i} \rho_{\text{HG}}(p_i, c_{t-1})$ ;
5      $c_t \leftarrow c_{t-1} \#_{1/(t+1)}^\rho p$ ;
6   Output  $c_T$ ;

```

---

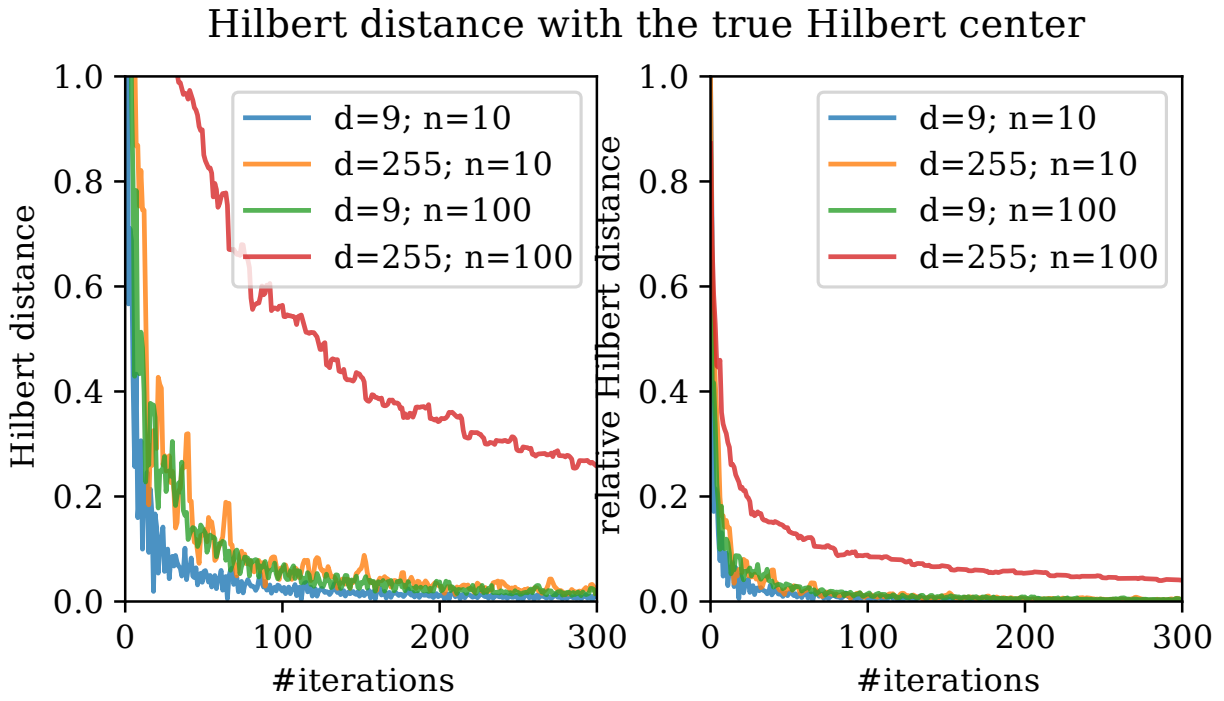


Figure 12: Convergence rate of Alg. (4) measured by the Hilbert distance between the current minimax center and the true center (left) or their Hilbert distance divided by the Hilbert radius of the dataset (right). The plot is based on 100 random points in  $\Delta^9/\Delta^{255}$ .

The algorithm first picks up a point  $c_0$  at random from  $\Lambda$  as the initial center, then computes the farthest point  $p$  (with respect to the distance  $\rho$ ), and then walk on the geodesic from  $c_0$  to  $p$  by a certain amount to define  $c_1$ , etc. For an arbitrary distance  $\rho$ , we define the operator  $\#_\alpha^\rho$  as follows:

$$p \#_\alpha^\rho q = v = \gamma(p, q, \alpha), \quad \rho(p : v) = \alpha \rho(p : q),$$

where  $\gamma(p, q, \alpha)$  is the geodesic passing through  $p$  and  $q$ , and parameterized by  $\alpha$  ( $0 \leq \alpha \leq 1$ ). When the equations of the geodesics are explicitly known, we can either get a closed form solution for  $\#_\alpha^\rho$  or perform a bisection search to

find  $v'$  such that  $\rho(p : v') \approx \alpha \rho(p : q)$ . See [54] for an extension and analysis in hyperbolic geometry. See Fig. (12) to get an intuitive idea on the *experimental* convergence rate of Algorithm 4. See Fig. (13) for visualizations of centers wrt different geometries.

Furthermore, this iterative algorithm implies a core-set [12] (namely, the set of farthest points visited during the geodesic walks) that is useful for clustering large data-sets [10]. See [18] for core-set results on containment problems wrt a convex homothetic object (the equivalent Hilbert polytope norm in our case).

A simple algorithm dubbed MINCON [67] can find an approximation of the Minimum Enclosing Polytope. The algorithm induces a core-set of size  $O(\frac{1}{\varepsilon^2})$  although the theorem is challenged in [18].

Thus by combining the  $k$ -center seeding [34] with the Lloyd-like batched iterations, we get an efficient  $k$ -center clustering algorithm for the FHR and Hilbert metric geometries. When dealing with the Kullback-Leibler divergence, we use the fact that KL is a Bregman divergence, and use the 1-center algorithm ([66, 57] for approximation in any dimension, or [58] which is exact but limited to small dimensions).

Since Hilbert simplex geometry is isomorphic to a normed vector space [46] with a polytope norm with  $d(d+1)$  facets, the Voronoi diagram in Hilbert geometry of  $\Delta^d$  amounts to compute a Voronoi diagram wrt a polytope norm [43, 72, 29].

## 5 Experiments

We generate a dataset consisting of a set of clusters in a high dimensional statistical simplex  $\Delta^d$ . Each cluster is generated independently as follows. We first pick a random center  $c = (\lambda_c^0, \dots, \lambda_c^d)$  based on the uniform distribution on  $\Delta^d$ . Then any random sample  $p = (\lambda^0, \dots, \lambda^d)$  associated with  $c$  is independently generated by

$$\lambda^i = \frac{\exp(\log \lambda_c^i + \sigma \varepsilon^i)}{\sum_{i=0}^d \exp(\log \lambda_c^i + \sigma \varepsilon^i)},$$

where  $\sigma > 0$  is a noise level parameter, and each  $\varepsilon^i$  follows independently a standard Gaussian distribution (generator 1) or the Student's  $t$ -distribution with five degrees of freedom (generator 2). Let  $\sigma = 0$ , we get  $\lambda^i = \lambda_c^i$ . Therefore  $p$  is randomly distributed around  $c$ . We repeat generating random samples for each cluster center, and make sure that different clusters have almost the same number of samples. Then we perform clustering based on the configurations  $n \in \{50, 100\}$ ,  $d \in \{9, 255\}$ ,  $\sigma \in \{0.5, 0.9\}$ ,  $\rho \in \{\rho_{\text{FHR}}, \rho_{\text{IG}}, \rho_{\text{HG}}, \rho_{\text{EUC}}, \rho_{\text{LI}}\}$ . For simplicity, the number of clusters  $k$  is set to the ground truth. For each configuration, we repeat the clustering experiment based on 300 different random datasets. The performance is measured by the normalized mutual information (NMI), which is a scalar indicator in the range  $[0, 1]$  (the larger the better).

The results of  $k$ -means++ and  $k$ -centers are shown in Table 2 and Table 3, respectively. The large variance of NMI is because that each experiment is performed on random datasets wrt different random seeds. Generally, the performance deteriorates as we increase the number of clusters, increase the noise level or decrease the dimensionality, which have the same effect to reduce the inter-cluster gap.

The key comparison is the three columns  $\rho_{\text{FHR}}$ ,  $\rho_{\text{HG}}$  and  $\rho_{\text{IG}}$ , as they are based on exactly the same algorithm with the only difference being the underlying geometry. We see clearly that in general, their clustering performance presents the order  $\text{HG} > \text{FHR} > \text{IG}$ . The performance of HG is superior to the other two geometries, especially when the noise level is large. Intuitively, the Hilbert balls are more compact in size and therefore can better capture the clustering structure (see Fig. (2)).

The column  $\rho_{\text{EUC}}$  is based on the Euclidean enclosing ball. It shows the worst scores because the intrinsic geometry of the probability simplex is far from the Euclidean geometry.

We also benchmark the  $k$ -means++ clustering on positive measures (not necessarily normalized). The experimental results are reported in Table 4.

## 6 Hilbert's projective geometry of the space of correlation matrices

In this section, we present the Hilbert's projective geometry to the space of correlation matrices

$$\mathcal{C}^d = \{C_{d \times d} : C \succ 0; C_{ii} = 1, \forall i\}.$$

Table 2:  $k$ -means++ clustering accuracy in NMI on randomly generated datasets based on different geometries. The table shows the mean and standard deviation after 300 independent runs for each configuration.  $\rho$  is the distance measure.  $n$  is the sample size.  $d$  is the dimensionality of  $\Delta^d$ .  $\sigma$  is noise level.

$k$	$n$	$d$	$\sigma$	$\rho_{\text{FHR}}$	$\rho_{\text{IG}}$	$\rho_{\text{HG}}$	$\rho_{\text{EUC}}$	$\rho_{L1}$
3	50	9	0.5	0.76 $\pm$ 0.22	0.76 $\pm$ 0.24	<b>0.81 <math>\pm</math> 0.22</b>	0.64 $\pm$ 0.23	0.70 $\pm$ 0.22
			0.9	0.44 $\pm$ 0.20	0.44 $\pm$ 0.20	<b>0.57 <math>\pm</math> 0.22</b>	0.31 $\pm$ 0.17	0.38 $\pm$ 0.18
		255	0.5	0.80 $\pm$ 0.24	0.81 $\pm$ 0.24	<b>0.88 <math>\pm</math> 0.21</b>	0.74 $\pm$ 0.25	0.79 $\pm$ 0.24
			0.9	0.65 $\pm$ 0.27	0.66 $\pm$ 0.28	<b>0.72 <math>\pm</math> 0.27</b>	0.46 $\pm$ 0.24	0.63 $\pm$ 0.27
	100	9	0.5	0.76 $\pm$ 0.22	0.76 $\pm$ 0.21	<b>0.82 <math>\pm</math> 0.22</b>	0.60 $\pm$ 0.21	0.69 $\pm$ 0.23
			0.9	0.42 $\pm$ 0.19	0.41 $\pm$ 0.18	<b>0.54 <math>\pm</math> 0.22</b>	0.27 $\pm$ 0.14	0.34 $\pm$ 0.16
		255	0.5	0.82 $\pm$ 0.23	0.82 $\pm$ 0.24	<b>0.89 <math>\pm</math> 0.20</b>	0.74 $\pm$ 0.24	0.80 $\pm$ 0.25
			0.9	0.66 $\pm$ 0.26	0.66 $\pm$ 0.28	<b>0.72 <math>\pm</math> 0.26</b>	0.45 $\pm$ 0.25	0.64 $\pm$ 0.27
5	50	9	0.5	0.75 $\pm$ 0.14	0.74 $\pm$ 0.15	<b>0.81 <math>\pm</math> 0.13</b>	0.61 $\pm$ 0.13	0.68 $\pm$ 0.13
			0.9	0.44 $\pm$ 0.13	0.42 $\pm$ 0.13	<b>0.55 <math>\pm</math> 0.15</b>	0.31 $\pm$ 0.11	0.36 $\pm$ 0.12
		255	0.5	0.83 $\pm$ 0.15	0.83 $\pm$ 0.15	<b>0.88 <math>\pm</math> 0.14</b>	0.77 $\pm$ 0.16	0.82 $\pm$ 0.15
			0.9	0.71 $\pm$ 0.17	0.70 $\pm$ 0.19	<b>0.75 <math>\pm</math> 0.17</b>	0.50 $\pm$ 0.17	0.68 $\pm$ 0.18
	100	9	0.5	0.74 $\pm$ 0.13	0.74 $\pm$ 0.14	<b>0.80 <math>\pm</math> 0.14</b>	0.60 $\pm$ 0.13	0.67 $\pm$ 0.13
			0.9	0.42 $\pm$ 0.11	0.40 $\pm$ 0.12	<b>0.55 <math>\pm</math> 0.15</b>	0.29 $\pm$ 0.09	0.35 $\pm$ 0.11
		255	0.5	0.83 $\pm$ 0.14	0.83 $\pm$ 0.15	<b>0.88 <math>\pm</math> 0.13</b>	0.77 $\pm$ 0.15	0.81 $\pm$ 0.15
			0.9	0.69 $\pm$ 0.18	0.69 $\pm$ 0.18	<b>0.73 <math>\pm</math> 0.17</b>	0.48 $\pm$ 0.17	0.67 $\pm$ 0.18

(a) generator 1

$k$	$n$	$d$	$\sigma$	$\rho_{\text{FHR}}$	$\rho_{\text{IG}}$	$\rho_{\text{HG}}$	$\rho_{\text{EUC}}$	$\rho_{L1}$
3	50	9	0.5	0.62 $\pm$ 0.22	0.60 $\pm$ 0.22	<b>0.71 <math>\pm</math> 0.23</b>	0.45 $\pm$ 0.20	0.54 $\pm$ 0.22
			0.9	0.29 $\pm$ 0.17	0.27 $\pm$ 0.16	<b>0.39 <math>\pm</math> 0.19</b>	0.17 $\pm$ 0.13	0.25 $\pm$ 0.15
		255	0.5	0.70 $\pm$ 0.25	0.69 $\pm$ 0.26	<b>0.74 <math>\pm</math> 0.25</b>	0.37 $\pm$ 0.29	0.70 $\pm$ 0.26
			0.9	<b>0.42 <math>\pm</math> 0.25</b>	0.35 $\pm$ 0.20	0.40 $\pm$ 0.19	0.03 $\pm$ 0.08	<b>0.44 <math>\pm</math> 0.26</b>
	100	9	0.5	0.63 $\pm$ 0.22	0.61 $\pm$ 0.22	<b>0.71 <math>\pm</math> 0.22</b>	0.46 $\pm$ 0.19	0.56 $\pm$ 0.20
			0.9	0.29 $\pm$ 0.15	0.26 $\pm$ 0.14	<b>0.38 <math>\pm</math> 0.20</b>	0.18 $\pm$ 0.12	0.24 $\pm$ 0.14
		255	0.5	0.71 $\pm$ 0.26	0.69 $\pm$ 0.27	<b>0.75 <math>\pm</math> 0.25</b>	0.31 $\pm$ 0.28	0.70 $\pm$ 0.27
			0.9	0.41 $\pm$ 0.26	0.33 $\pm$ 0.20	0.38 $\pm$ 0.18	0.02 $\pm$ 0.06	<b>0.43 <math>\pm</math> 0.26</b>
5	50	9	0.5	0.64 $\pm$ 0.15	0.61 $\pm$ 0.14	<b>0.70 <math>\pm</math> 0.14</b>	0.48 $\pm$ 0.14	0.57 $\pm$ 0.15
			0.9	0.31 $\pm$ 0.12	0.29 $\pm$ 0.12	<b>0.41 <math>\pm</math> 0.15</b>	0.20 $\pm$ 0.09	0.26 $\pm$ 0.10
		255	0.5	0.74 $\pm$ 0.17	0.72 $\pm$ 0.17	<b>0.77 <math>\pm</math> 0.16</b>	0.41 $\pm$ 0.20	0.74 $\pm$ 0.17
			0.9	0.44 $\pm$ 0.17	0.37 $\pm$ 0.16	0.44 $\pm$ 0.15	0.04 $\pm$ 0.06	<b>0.47 <math>\pm</math> 0.17</b>
	100	9	0.5	0.62 $\pm$ 0.14	0.61 $\pm$ 0.14	<b>0.71 <math>\pm</math> 0.14</b>	0.46 $\pm$ 0.13	0.54 $\pm$ 0.14
			0.9	0.30 $\pm$ 0.10	0.27 $\pm$ 0.11	<b>0.40 <math>\pm</math> 0.13</b>	0.19 $\pm$ 0.08	0.25 $\pm$ 0.09
		255	0.5	0.73 $\pm$ 0.18	0.70 $\pm$ 0.18	<b>0.75 <math>\pm</math> 0.16</b>	0.37 $\pm$ 0.20	0.73 $\pm$ 0.17
			0.9	0.43 $\pm$ 0.16	0.35 $\pm$ 0.14	0.41 $\pm$ 0.12	0.03 $\pm$ 0.06	<b>0.46 <math>\pm</math> 0.18</b>

(b) generator 2

Table 3:  $k$ -center clustering accuracy in NMI on randomly generated datasets based on different geometries. The table shows the mean and standard deviation after 300 independent runs for each configuration.  $\rho$  is the distance measure.  $n$  is the sample size.  $d$  is the dimensionality of the statistical simplex.  $\sigma$  is noise level.

$k$	$n$	$d$	$\sigma$	$\rho_{\text{FHR}}$	$\rho_{\text{IG}}$	$\rho_{\text{HG}}$	$\rho_{\text{EUC}}$	$\rho_{\text{L1}}$
3	50	9	0.5	0.87 ± 0.19	0.85 ± 0.19	<b>0.92 ± 0.16</b>	0.72 ± 0.22	0.80 ± 0.20
			0.9	0.54 ± 0.21	0.51 ± 0.21	<b>0.70 ± 0.23</b>	0.36 ± 0.17	0.44 ± 0.19
		255	0.5	0.93 ± 0.16	0.92 ± 0.18	<b>0.95 ± 0.14</b>	0.89 ± 0.18	0.90 ± 0.19
			0.9	0.76 ± 0.24	0.72 ± 0.26	<b>0.82 ± 0.24</b>	0.50 ± 0.28	0.76 ± 0.25
	100	9	0.5	0.88 ± 0.17	0.86 ± 0.18	<b>0.93 ± 0.14</b>	0.70 ± 0.20	0.80 ± 0.20
			0.9	0.53 ± 0.20	0.49 ± 0.19	<b>0.70 ± 0.22</b>	0.33 ± 0.14	0.41 ± 0.18
		255	0.5	0.93 ± 0.16	0.92 ± 0.17	<b>0.95 ± 0.13</b>	0.88 ± 0.19	0.93 ± 0.16
			0.9	0.81 ± 0.22	0.75 ± 0.24	<b>0.83 ± 0.22</b>	0.47 ± 0.28	0.79 ± 0.22
5	50	9	0.5	0.82 ± 0.13	0.81 ± 0.13	<b>0.89 ± 0.12</b>	0.67 ± 0.13	0.75 ± 0.13
			0.9	0.50 ± 0.13	0.47 ± 0.13	<b>0.66 ± 0.15</b>	0.34 ± 0.11	0.40 ± 0.12
		255	0.5	<b>0.92 ± 0.11</b>	<b>0.91 ± 0.12</b>	<b>0.93 ± 0.11</b>	0.87 ± 0.13	<b>0.92 ± 0.12</b>
			0.9	0.77 ± 0.15	0.71 ± 0.17	<b>0.85 ± 0.17</b>	0.54 ± 0.19	0.74 ± 0.16
	100	9	0.5	0.83 ± 0.12	0.81 ± 0.13	<b>0.89 ± 0.11</b>	0.67 ± 0.11	0.76 ± 0.13
			0.9	0.48 ± 0.12	0.46 ± 0.12	<b>0.66 ± 0.15</b>	0.33 ± 0.09	0.39 ± 0.10
		255	0.5	<b>0.93 ± 0.10</b>	<b>0.92 ± 0.11</b>	<b>0.94 ± 0.09</b>	0.89 ± 0.11	0.92 ± 0.11
			0.9	0.81 ± 0.14	0.74 ± 0.15	<b>0.84 ± 0.16</b>	0.52 ± 0.19	0.79 ± 0.14

(a) generator 1

$k$	$n$	$d$	$\sigma$	$\rho_{\text{FHR}}$	$\rho_{\text{IG}}$	$\rho_{\text{HG}}$	$\rho_{\text{EUC}}$	$\rho_{\text{L1}}$
3	50	9	0.5	0.68 ± 0.22	0.67 ± 0.22	<b>0.80 ± 0.20</b>	0.48 ± 0.22	0.60 ± 0.22
			0.9	0.32 ± 0.18	0.29 ± 0.17	<b>0.45 ± 0.21</b>	0.20 ± 0.14	0.26 ± 0.15
		255	0.5	0.79 ± 0.24	0.75 ± 0.24	<b>0.82 ± 0.22</b>	0.13 ± 0.23	<b>0.81 ± 0.24</b>
			0.9	0.35 ± 0.27	0.35 ± 0.21	<b>0.42 ± 0.19</b>	0.00 ± 0.02	0.32 ± 0.30
	100	9	0.5	0.66 ± 0.22	0.65 ± 0.22	<b>0.79 ± 0.21</b>	0.45 ± 0.19	0.59 ± 0.20
			0.9	0.30 ± 0.16	0.28 ± 0.14	<b>0.42 ± 0.19</b>	0.20 ± 0.12	0.26 ± 0.14
		255	0.5	0.78 ± 0.25	0.76 ± 0.24	<b>0.82 ± 0.21</b>	0.05 ± 0.14	0.77 ± 0.27
			0.9	0.29 ± 0.28	0.29 ± 0.20	<b>0.39 ± 0.20</b>	0.00 ± 0.02	0.22 ± 0.25
5	50	9	0.5	0.69 ± 0.14	0.66 ± 0.14	<b>0.77 ± 0.13</b>	0.50 ± 0.13	0.61 ± 0.14
			0.9	0.34 ± 0.12	0.30 ± 0.12	<b>0.46 ± 0.15</b>	0.22 ± 0.09	0.28 ± 0.10
		255	0.5	<b>0.80 ± 0.15</b>	0.76 ± 0.15	<b>0.82 ± 0.14</b>	0.24 ± 0.23	<b>0.81 ± 0.14</b>
			0.9	0.42 ± 0.21	0.38 ± 0.16	<b>0.46 ± 0.15</b>	0.00 ± 0.02	0.39 ± 0.22
	100	9	0.5	0.66 ± 0.13	0.64 ± 0.14	<b>0.77 ± 0.14</b>	0.47 ± 0.13	0.57 ± 0.13
			0.9	0.31 ± 0.11	0.28 ± 0.10	<b>0.44 ± 0.13</b>	0.21 ± 0.08	0.25 ± 0.09
		255	0.5	<b>0.80 ± 0.16</b>	0.76 ± 0.15	<b>0.82 ± 0.13</b>	0.12 ± 0.17	<b>0.81 ± 0.16</b>
			0.9	0.32 ± 0.19	0.30 ± 0.15	<b>0.41 ± 0.13</b>	0.00 ± 0.01	0.26 ± 0.18

(b) generator 2

Table 4: kmeans++ clustering of  $N = 50$  random samples in  $\Delta^9$ .  $k$  is the ground truth number of clusters ,  $\sigma$  is noise level, For each configuration we repeat 300 runs and report the NMI score.

$k$	$\sigma$	$\rho_{\text{IG}}$	$\rho_{\text{FHR}}$	$\rho_{\text{HG}}$	$\rho_{\text{BG}}$
3	0.5	0.76 ± 0.23	0.76 ± 0.23	<b>0.85 ± 0.21</b>	<b>0.84 ± 0.21</b>
3	0.9	0.42 ± 0.20	0.45 ± 0.19	0.57 ± 0.23	<b>0.60 ± 0.22</b>
5	0.5	0.76 ± 0.14	0.74 ± 0.14	<b>0.80 ± 0.14</b>	<b>0.81 ± 0.14</b>
5	0.9	0.41 ± 0.12	0.44 ± 0.13	<b>0.55 ± 0.15</b>	<b>0.55 ± 0.15</b>

Table 5: NMI (mean $\pm$ std) of  $k$ -means++ clustering based on different distance measures in the ellipope (500 independent runs)

$v_1$	$v_2$	$\rho_{\text{HG}}$	$\rho_{\text{EUC}}$	$\rho_{\text{L1}}$	$\rho_{\text{LD}}$
4	10	<b>0.62 <math>\pm</math> 0.22</b>	0.57 $\pm$ 0.21	0.56 $\pm$ 0.22	0.58 $\pm$ 0.22
4	30	<b>0.85 <math>\pm</math> 0.18</b>	0.80 $\pm$ 0.20	0.81 $\pm$ 0.19	0.82 $\pm$ 0.20
4	50	<b>0.89 <math>\pm</math> 0.17</b>	0.87 $\pm$ 0.17	0.86 $\pm$ 0.18	0.88 $\pm$ 0.18
5	10	<b>0.50 <math>\pm</math> 0.21</b>	0.49 $\pm$ 0.21	0.48 $\pm$ 0.20	0.47 $\pm$ 0.21
5	30	<b>0.77 <math>\pm</math> 0.20</b>	0.75 $\pm$ 0.21	0.75 $\pm$ 0.21	0.75 $\pm$ 0.21
5	50	<b>0.84 <math>\pm</math> 0.19</b>	0.82 $\pm$ 0.19	0.82 $\pm$ 0.20	<b>0.84 <math>\pm</math> 0.18</b>

If  $C_1, C_2 \in \mathcal{C}$ , then  $(1 - \lambda)C_1 + \lambda C_2 \in \mathcal{C}$  for  $0 < \lambda < 1$ . Therefore  $\mathcal{C}$  is a convex set, known as an *ellipope* [81] embedded in the p.s.d. cone. See Fig. (14) for an intuitive view of  $\mathcal{C}_3$ , where the coordinate system  $(x, y, z)$  is the off-diagonal entries of  $C \in \mathcal{C}_3$ .

In order to compute the Hilbert distance  $\rho_{\text{HG}}(C_1, C_2)$ , we need to compute the intersection of the line  $(C_1, C_2)$  with  $\partial\mathcal{C}$ , denoted as  $C'_1$  and  $C'_2$ , then we have

$$\rho_{\text{HG}}(C_1, C_2) = \left| \log \frac{\|C_1 - C'_2\| \|C'_1 - C_2\|}{\|C_1 - C'_1\| \|C_2 - C'_2\|} \right|.$$

Unfortunately there is no closed form solution of  $C'_1$  and  $C'_2$ . Instead, we apply a binary searching algorithm. Note a necessary condition for  $C \in \mathcal{C}$  is that  $C$  has a positive spectrum. If  $C$  has at least one non-positive eigenvalue, then  $C \notin \mathcal{C}$ . To determine whether a given  $C$  is inside the ellipope requires a spectral decomposition of  $C$ . Therefore the computation of  $C'_1$  and  $C'_2$  is in general expensive.

We compare the Hilbert ellipope geometry with commonly used distance measures including the  $L_2$  distance  $\rho_{\text{EUC}}$ ,  $L_1$  distance  $\rho_{\text{L1}}$ , and the square root of the log-det divergence

$$\rho_{\text{LD}}(C_1, C_2) = \text{tr}(C_1 C_2^{-1}) - \log |C_1 C_2^{-1}| - d.$$

Due to the high computational complexity, we only investigate  $k$ -means++ clustering. The investigated dataset consists of 100 matrices forming 3 clusters in  $\mathcal{C}_3$  with almost identical size. Each cluster is independently generated according to

$$P \sim \mathcal{W}^{-1}(I_{3 \times 3}, v_1), \\ C_i \sim \mathcal{W}^{-1}(P, v_2),$$

where  $\mathcal{W}^{-1}(A, v)$  denotes the inverse Wishart distribution with scale matrix  $A$  and  $v$  degrees of freedom, and  $C_i$  is a point in the cluster associated with  $P$ . Table 5 shows the  $k$ -means++ clustering performance in terms of NMI. Again Hilbert geometry is favorable as compared to alternatives, showing that the good performance of Hilbert clustering is generalizable.

We also consider the *Thompson metric distance* [47] defined over the cone of positive-semidefinite matrices:

$$\rho_{\text{TG}}(P, Q) := \max_i |\log \lambda_i(P^{-1}Q)|. \quad (15)$$

We observe experimentally that the symmetric KL or KL(selected cluster centers:other points) is better than the Thompson metric and KL(other points:selected cluster centers).

## 7 Conclusion

We introduced the Hilbert (projective) metric distance and its underlying non-Riemannian geometry for modeling the space of multinomials or the open probability simplex. We compared experimentally in simulated clustering tasks this

geometry with the traditional differential geometric modelings (either the Fisher-Hotelling-Rao metric connection or the dually coupled non-metric affine connections of information geometry [4]).

The main feature of Hilbert geometry (HG) is that it is a metric non-manifold geometry, where geodesics are straight (Euclidean) line segments. This makes this geometry computationally attractive. In simplex domains, the Hilbert balls have fixed combinatorial (Euclidean) polytope structures, and HG is known to be isometric to a normed space [28, 33]. This latter isometry allows one to generalize easily the standard proofs of clustering (*e.g.*,  $k$ -means or  $k$ -center). We demonstrated it for the  $k$ -means++ competitive performance analysis and for the convergence of the 1-center heuristic [11] (smallest enclosing Hilbert ball allows one to implement efficiently the  $k$ -center clustering). Our experimental  $k$ -means++ or  $k$ -center comparisons of HG algorithms with the manifold modeling approach yield superior performance. This may be intuitively explained by the sharpness of Hilbert balls as compared to the FHR/IG ball profiles. However, when considering the Hilbert simplex geometry, let us notice that we do not get a Busemann's geodesic space [20] (Busemann G-space) since the region

$$R(p, q) = \{r : \rho_{\text{HG}}(p, q) = \rho_{\text{HG}}(p, r) + \rho_{\text{HG}}(q, r)\}, \quad (16)$$

defining the locii of point  $r$  such that triples  $(p, r, q)$  satisfies the triangle equality is *not* a line segment but the intersection of cones [28]. We proved that the Hilbert simplex geometry satisfies the property of information monotonicity (Theorem 2) albeit being non-separable, a key requirement in information geometry [4]. The automorphism group (group of motions) of the Hilbert simplex geometry is reported in [28].

Chentsov [24] defined statistical invariance on a probability manifold under Markov morphisms and proved that the Fisher Information Metric is the unique Riemannian metric (up to rescaling) for multinomials. However, this does not rule out that other distances (with underlying geometric structures) may be used to model statistical manifolds (*e.g.*, Finsler statistical manifolds [23, 77], or the total variation distance — the only metric  $f$ -divergence [42]). Defining statistical invariance related to geometry is the cornerstone problem of information geometry that can be tackled from many directions (see [31] and references therein for a short review). The Hilbert cross-ratio metric is by construction invariant to the group of collineations.

In this paper, we introduced Hilbert geometries in machine learning by considering clustering tasks in the probability simplex and in the correlation ellipope. A canonical Hilbert metric distance can be defined on any bounded convex subset of the Euclidean space with the key property that geodesics are straight Euclidean line segments thus making this geometry well-suited for fast and exact computations. Thus we may consider clustering in other bounded convex subsets like the simplices [30].

One future direction is to consider the Hilbert metric for regularization and sparsity in machine learning (due to its equivalence with a polytope normed distance).

Our Python codes are freely available online for reproducible research:

<https://franknielsen.github.io/HSG/>

## References

- [1] Marcel R Ackermann and Johannes Blömer. Bregman clustering for separable instances. In *Scandinavian Workshop on Algorithm Theory*, pages 212–223. Springer, 2010.
- [2] Charu C. Aggarwal and Cheng Xiang Zhai. *Mining Text Data*. Springer Publishing Company, 2012.
- [3] Alan Agresti. *Categorical data analysis*, volume 482. John Wiley & Sons, 2003.
- [4] Shun-ichi Amari. *Information Geometry and Its Applications*, volume 194 of *Applied Mathematical Sciences*. Springer Japan, 2016.
- [5] Shun-ichi Amari and Andrzej Cichocki. Information geometry of divergence functions. *Bulletin of the Polish Academy of Sciences: Technical Sciences*, 58(1):183–195, 2010.
- [6] Marc Arnaudon and Frank Nielsen. Medians and means in Finsler geometry. *LMS Journal of Computation and Mathematics*, 15:23–37, 2012.

- [7] Marc Arnaudon and Frank Nielsen. On approximating the Riemannian 1-center. *Computational Geometry*, 46(1):93–104, 2013.
- [8] David Arthur and Sergei Vassilvitskii.  $k$ -means++: The advantages of careful seeding. In *ACM-SIAM Symposium on Discrete Algorithms (SODA)*, pages 1027–1035, 2007.
- [9] Olivier Bachem, Mario Lucic, S. Hamed Hassani, and Andreas Krause. Approximate  $k$ -means++ in sublinear time. In *Proceedings of the Thirtieth AAAI Conference on Artificial Intelligence*, pages 1459–1467, 2016.
- [10] Olivier Bachem, Mario Lucic, and Andreas Krause. Scalable and distributed clustering via lightweight coresets, 2017. arXiv:1702.08248 [stat.ML].
- [11] Mihai Bădoiu and Kenneth L. Clarkson. Smaller core-sets for balls. In *ACM-SIAM Symposium on Discrete Algorithms (SODA)*, pages 801–802, 2003.
- [12] Mihai Bădoiu and Kenneth L Clarkson. Optimal core-sets for balls. *Computational Geometry*, 40(1):14–22, 2008.
- [13] Ingemar Bengtsson and Karol Zyczkowski. *Geometry of quantum states: An introduction to quantum entanglement*. Cambridge university press, 2017.
- [14] Andreas Bernig. Hilbert geometry of polytopes. *Archiv der Mathematik*, 92(4):314–324, 2009.
- [15] Yanhong Bi, Bin Fan, and Fuchao Wu. Beyond Mahalanobis metric: Cayley-Klein metric learning. In *IEEE Conference on Computer Vision and Pattern Recognition (CVPR)*, pages 2339–2347, 2015.
- [16] Garrett Birkhoff. Extensions of Jentzschs theorem. *Transactions of the American Mathematical Society*, 85(1):219–227, 1957.
- [17] J-D Boissonnat, Micha Sharir, Boaz Tagansky, and Mariette Yvinec. Voronoi diagrams in higher dimensions under certain polyhedral distance functions. *Discrete & Computational Geometry*, 19(4):485–519, 1998.
- [18] René Brandenberg and Stefan König. No dimension-independent core-sets for containment under homothetics. *Discrete & Computational Geometry*, 49(1):3–21, 2013.
- [19] Herbert Busemann. *The Geometry of Geodesics*, volume 6 of *Pure and Applied Mathematics*. Elsevier Science, 1955.
- [20] Herbert Busemann. *The geometry of geodesics*. Pure and applied mathematics. Academic Press, 1955.
- [21] Herbert Busemann and Paul J Kelly. *Projective geometry and projective metrics*. Courier Corporation, 2012.
- [22] Ovidiu Calin and Constantin Udriste. *Geometric Modeling in Probability and Statistics*. Mathematics and Statistics. Springer International Publishing, 2014.
- [23] Alberto Cena. *Geometric structures on the non-parametric statistical manifold*. PhD thesis, University of Milano, 2002.
- [24] N. N. Cencov. *Statistical Decision Rules and Optimal Inference*, volume 53 of *Translations of mathematical monographs*. American Mathematical Society, 2000.
- [25] Douglas G Chapman and Herbert Robbins. Minimum variance estimation without regularity assumptions. *The Annals of Mathematical Statistics*, pages 581–586, 1951.
- [26] Kamalika Chaudhuri and Andrew McGregor. Finding metric structure in information theoretic clustering. In *Conference on Learning Theory (COLT)*, pages 391–402, 2008.
- [27] Laurent Condat. Fast projection onto the simplex and the  $\ell_1$  ball. *Mathematical Programming*, 158(1-2):575–585, 2016.

- [28] Pierre de la Harpe. On Hilbert’s metric for simplices. In *Geometric Group Theory*, volume 1, pages 97–118. Cambridge Univ. Press, 1991.
- [29] Michel Deza and Mathieu Dutour Sikirić. Voronoi polytopes for polyhedral norms on lattices. *Discrete Applied Mathematics*, 197:42–52, 2015.
- [30] Timothy M Doup. *Simplicial algorithms on the simplotope*, volume 318. Springer Science & Business Media, 2012.
- [31] James G. Dowty. Chentsov’s theorem for exponential families, 2017. arXiv:1701.08895 [math.ST].
- [32] Yasunori Endo and Sadaaki Miyamoto. Spherical  $k$ -means++ clustering. In *Modeling Decisions for Artificial Intelligence*, pages 103–114. Springer, 2015.
- [33] Thomas Foertsch and Anders Karlsson. Hilbert metrics and Minkowski norms. *Journal of Geometry*, 83(1–2):22–31, 2005.
- [34] Teofilo F Gonzalez. Clustering to minimize the maximum intercluster distance. *Theoretical Computer Science*, 38:293–306, 1985.
- [35] JM Hammersley. On estimating restricted parameters. *Journal of the Royal Statistical Society. Series B (Methodological)*, 12(2):192–240, 1950.
- [36] David Hilbert. Über die gerade linie als kürzeste verbindung zweier punkte. *Mathematische Annalen*, 46(1):91–96, 1895.
- [37] Harold Hotelling. Spaces of statistical parameters. In *Bulletin AMS*, volume 36, page 191, 1930.
- [38] Zhexue Huang. Extensions to the  $k$ -means algorithm for clustering large data sets with categorical values. *Data mining and knowledge discovery*, 2(3):283–304, 1998.
- [39] Robert Jenssen, Jose C Principe, Deniz Erdogmus, and Torbjørn Eltoft. The Cauchy-Schwarz divergence and Parzen windowing: Connections to graph theory and mercer kernels. *Journal of the Franklin Institute*, 343(6):614–629, 2006.
- [40] Jiantao Jiao, Thomas A Courtade, Albert No, Kartik Venkat, and Tsachy Weissman. Information measures: the curious case of the binary alphabet. *IEEE Transactions on Information Theory*, 60(12):7616–7626, 2014.
- [41] Robert E. Kass and Paul W. Vos. *Geometrical Foundations of Asymptotic Inference*. Wiley Series in Probability and Statistics. Wiley-Interscience, 1997.
- [42] Mohammadali Khosravifard, Dariush Fooladivanda, and T Aaron Gulliver. Confliction of the convexity and metric properties in  $f$ -divergences. *IEICE Transactions on Fundamentals of Electronics, Communications and Computer Sciences*, 90(9):1848–1853, 2007.
- [43] Mark-Christoph Körner. *Minisum hyperspheres*, volume 51 of *Springer Optimization and Its Applications*. Springer New York, 2011.
- [44] David H Laidlaw and Joachim Weickert. *Visualization and Processing of Tensor Fields: Advances and Perspectives*. Mathematics and Visualization. Springer-Verlag Berlin Heidelberg, 2009.
- [45] Guy Lebanon. Learning Riemannian metrics. In *Conference on Uncertainty in Artificial Intelligence (UAI)*, pages 362–369, 2002.
- [46] Bas Lemmens and Roger Nussbaum. Birkhoff’s version of Hilbert’s metric and its applications in analysis. *Handbook of Hilbert Geometry*, pages 275–303, 2014.
- [47] Bas Lemmens, Mark Roelands, et al. Midpoints for Thompson’s metric on symmetric cones. *Osaka Journal of Mathematics*, 54(1):197–208, 2017.

- [48] Bas Lemmens and Cormac Walsh. Isometries of polyhedral Hilbert geometries. *Journal of Topology and Analysis*, 3(02):213–241, 2011.
- [49] Xiao Liang. A note on divergences. *Neural Computation*, 28(10):2045–2062, 2016.
- [50] Bodo Manthey and Heiko Röglin. Worst-case and smoothed analysis of  $k$ -means clustering with Bregman divergences. *Journal of Computational Geometry*, 4(1):94–132, 2013.
- [51] Ross Messing, Chris Pal, and Henry Kautz. Activity recognition using the velocity histories of tracked keypoints. In *International Conference on Computer Vision*, pages 104–111. IEEE, 2009.
- [52] Kevin P. Murphy. *Machine Learning: A Probabilistic Perspective*. The MIT Press, 2012.
- [53] Frank Nielsen. Cramér-Rao lower bound and information geometry. In *Connected at Infinity II*, pages 18–37. Springer, 2013.
- [54] Frank Nielsen and Gaëtan Hadjeres. Approximating covering and minimum enclosing balls in hyperbolic geometry. In *International Conference on Networked Geometric Science of Information*, pages 586–594. Springer, 2015.
- [55] Frank Nielsen, Boris Muzellec, and Richard Nock. Classification with mixtures of curved Mahalanobis metrics. In *IEEE International Conference on Image Processing (ICIP)*, pages 241–245, 2016.
- [56] Frank Nielsen, Boris Muzellec, and Richard Nock. Large margin nearest neighbor classification using curved Mahalanobis distances, 2016. arXiv:1609.07082 [cs.LG].
- [57] Frank Nielsen and Richard Nock. On approximating the smallest enclosing Bregman balls. In *Proceedings of the twenty-second annual symposium on Computational geometry*, pages 485–486. ACM, 2006.
- [58] Frank Nielsen and Richard Nock. On the smallest enclosing information disk. *Information Processing Letters*, 105(3):93–97, 2008.
- [59] Frank Nielsen and Richard Nock. Approximating smallest enclosing balls with applications to machine learning. *International Journal of Computational Geometry & Applications*, 19(05):389–414, 2009.
- [60] Frank Nielsen and Richard Nock. Total Jensen divergences: Definition, properties and  $k$ -means++ clustering, 2013. arXiv:1309.7109 [cs.IT].
- [61] Frank Nielsen and Richard Nock. Further heuristics for  $k$ -means: The merge-and-split heuristic and the  $(k, l)$ -means. arXiv:1406.6314, 2014.
- [62] Frank Nielsen, Richard Nock, and Shun-ichi Amari. On clustering histograms with  $k$ -means by using mixed  $\alpha$ -divergences. *Entropy*, 16(6):3273–3301, 2014.
- [63] Frank Nielsen and Laëtitia Shao. On balls in a polygonal Hilbert geometry. In *33st International Symposium on Computational Geometry (SoCG 2017)*. Schloss Dagstuhl–Leibniz-Zentrum fuer Informatik, 2017.
- [64] Frank Nielsen and Ke Sun. Clustering in Hilbert simplex geometry. *CoRR*, abs/1704.00454, 2017.
- [65] Frank Nielsen, Ke Sun, and Stéphane Marchand-Maillet. On Hölder projective divergences. *Entropy*, 19(3), 2017.
- [66] Richard Nock and Frank Nielsen. Fitting the smallest enclosing Bregman ball. In *ECML*, pages 649–656. Springer, 2005.
- [67] Rina Panigrahy. Minimum enclosing polytope in high dimensions, 2004. arXiv:cs/0407020 [cs.CG].
- [68] Athanase Papadopoulos and Marc Troyanov. From Funk to Hilbert geometry, 2014. arXiv:1406.6983 [math.MG].

- [69] Poo-Sung Park. Regular polytopic distances. In *Forum Geometricorum*, volume 16, pages 227–232, 2016.
- [70] C Radhakrishna Rao. Information and accuracy attainable in the estimation of statistical parameters. *Bull. Cal. Math. Soc.*, 37(3):81–91, 1945.
- [71] C Radhakrishna Rao. Information and the accuracy attainable in the estimation of statistical parameters. In *Breakthroughs in statistics*, pages 235–247. Springer, 1992.
- [72] Daniel Reem. The geometric stability of Voronoi diagrams in normed spaces which are not uniformly convex, 2012. arXiv:1212.1094 [cs.CG].
- [73] Jürgen Richter-Gebert. *Perspectives on projective geometry: A guided tour through real and complex geometry*. Springer-Verlag Berlin Heidelberg, 2011.
- [74] Loïs Rigouste, Olivier Cappé, and François Yvon. Inference and evaluation of the multinomial mixture model for text clustering. *Information processing & management*, 43(5):1260–1280, 2007.
- [75] Ankan Saha, SVN Vishwanathan, and Xinhua Zhang. New approximation algorithms for minimum enclosing convex shapes. In *ACM-SIAM Symposium on Discrete Algorithms (SODA)*, pages 1146–1160, 2011.
- [76] Micha Sharir and Emo Welzl. A combinatorial bound for linear programming and related problems. *STACS 92*, pages 567–579, 1992.
- [77] Zhongmin Shen. Riemann-Finsler geometry with applications to information geometry. *Chinese Annals of Mathematics-Series B*, 27(1):73–94, 2006.
- [78] Hirohiko Shima. *The Geometry of Hessian Structures*. World Scientific, 2007.
- [79] Stephen M Stigler et al. The epic story of maximum likelihood. *Statistical Science*, 22(4):598–620, 2007.
- [80] John Stillwell. Ideal elements in Hilbert’s geometry. *Perspectives on Science*, 22(1):35–55, 2014.
- [81] Joel A Tropp. Simplicial faces of the set of correlation matrices. *Discrete & Computational Geometry*, 60(2):512–529, 2018.
- [82] Constantin Vernicos. Introduction aux géométries de Hilbert. *Séminaire de théorie spectrale et géométrie*, 23:145–168, 2004.
- [83] Emo Welzl. Smallest enclosing disks (balls and ellipsoids). *New results and new trends in computer science*, pages 359–370, 1991.

## A Isometry of Hilbert simplex geometry to a normed vector space

Consider the Hilbert simplex metric space  $(\Delta^d, \rho_{\text{HG}})$  where  $\Delta^d$  denotes the  $d$ -dimensional open probability simplex and  $\rho_{\text{HG}}$  the Hilbert cross-ratio metric. Let us recall the isometry ([28], 1991) of the open standard simplex to a normed vector space  $(V^d, \|\cdot\|_{\text{NH}})$ . Let  $V^d = \{v \in \mathbb{R}^{d+1} : \sum_i v^i = 0\}$  denote the  $d$ -dimensional vector space sitting in  $\mathbb{R}^{d+1}$ . Map a point  $p = (\lambda^0, \dots, \lambda^d) \in \Delta^d$  to a point  $v(x) = (v^0, \dots, v^d) \in V^d$  as follows:

$$v^i = \frac{1}{d+1} \left( d \log \lambda^i - \sum_{j \neq i} \log \lambda^j \right) = \log \lambda^i - \frac{1}{d+1} \sum_j \log \lambda^j.$$

We define the corresponding norm  $\|\cdot\|_{\text{NH}}$  in  $V^d$  by considering the shape of its unit ball  $B_V = \{v \in V^d : |v^i - v^j| \leq 1, \forall i \neq j\}$ . The unit ball  $B_V$  is a symmetric convex set containing the origin in its interior, and thus yields a *polytope norm*  $\|\cdot\|_{\text{NH}}$  (Hilbert norm) with  $2 \binom{d+1}{2} = d(d+1)$  facets. Reciprocally, let us notice that a norm induces a unit ball centered at the origin that is convex and symmetric around the origin.

The distance in the normed vector space between  $v \in V^d$  and  $v' \in V^d$  is defined by:

$$\rho_V(v, v') = \|v - v'\|_{\text{NH}} = \inf \{\tau : v' \in \tau(B_V \oplus \{v\})\},$$

where  $A \oplus B = \{a + b : a \in A, b \in B\}$  is the Minkowski sum.

The reverse map from the normed space  $V^d$  to the probability simplex  $\Delta^d$  is given by:

$$\lambda^i = \frac{\exp(v^i)}{\sum_j \exp(v^j)}.$$

Thus we have  $(\Delta^d, \rho_{\text{HG}}) \cong (V^d, \|\cdot\|_{\text{NH}})$ . In 1D,  $(V^1, \|\cdot\|_{\text{NH}})$  is isometric to the Euclidean line.

Note that computing the distance in the normed vector space requires naively  $O(d^2)$  time.

Unfortunately, the norm  $\|\cdot\|_{\text{NH}}$  does not satisfy the parallelogram law.<sup>4</sup> Notice that a norm satisfying the parallelogram law can be associated with an inner product via the polarization identity. Thus the isometry of the Hilbert geometry to a normed vector space is not equipped with an inner product. However, all norms in a finite dimensional space are equivalent. This implies that in finite dimension,  $(\Delta^d, \rho_{\text{HG}})$  is *quasi-isometric* to the Euclidean space  $\mathbb{R}^d$ . An example of Hilbert geometry in infinite dimension is reported in [28]. Hilbert spaces are not CAT spaces except when  $\mathcal{C}$  is an ellipsoid [82].

## B Hilbert geometry with Finslerian/Riemannian structures

In a Riemannian geometry, each tangent plane  $T_p M$  of a  $d$ -dimensional manifold  $M$  is equivalent to  $\mathbb{R}^d$ :  $T_p M \simeq \mathbb{R}^d$ . The inner product at each tangent plane  $T_p M$  can be visualized by an ellipsoid shape, a convex symmetric object centered at point  $p$ . In a *Finslerian geometry*, a norm  $\|\cdot\|_p$  is defined in each tangent plane  $T_p M$ , and this norm is visualized as a symmetric convex object with non-empty interior. Finslerian geometry thus generalizes Riemannian geometry by taking into account generic symmetric convex objects instead of ellipsoids for inducing norms at each tangent plane. Any Hilbert geometry induced by a compact convex domain  $\mathcal{C}$  can be expressed by an equivalent Finslerian geometry by defining the norm in  $T_p$  at  $p$  as follows [82]:

$$\|v\|_p = F_{\mathcal{C}}(p, v) = \frac{\|v\|}{2} \left( \frac{1}{pp^+} + \frac{1}{pp^-} \right),$$

where  $F_{\mathcal{C}}$  is the *Finsler metric*,  $\|\cdot\|$  is an *arbitrary norm* on  $\mathbb{R}^d$ , and  $p^+$  and  $p^-$  are the intersection points of the line passing through  $p$  with direction  $v$ :

$$p^+ = p + t^+ v, \quad p^- = p + t^- v.$$

A geodesic  $\gamma$  in a Finslerian geometry satisfies:

$$d_{\mathcal{C}}(\gamma(t_1), \gamma(t_2)) = \int_{t_1}^{t_2} F_{\mathcal{C}}(\gamma(t), \dot{\gamma}(t)) dt.$$

In  $T_p M$ , a ball of center  $c$  and radius  $r$  is defined by:

$$B(c, r) = \{v : F_{\mathcal{C}}(c, v) \leq r\}.$$

Thus any Hilbert geometry induces an equivalent Finslerian geometry, and since Finslerian geometries include Riemannian geometries, one may wonder which Hilbert geometries induce Riemannian structures? The only Riemannian geometries induced by Hilbert geometries are the *hyperbolic Cayley-Klein geometries* [73, 56, 55] with the domain  $\mathcal{C}$  being an ellipsoid. The Finslerian modeling of information geometry has been studied in [23, 77].

There is not a canonical way of defining measures in a Hilbert geometry since Hilbert geometries are Finslerian but not necessary Riemannian geometries [82]. The Busemann measure is defined according to the Lebesgue measure

---

<sup>4</sup>Consider  $A = (1/3, 1/3, 1/3)$ ,  $B = (1/6, 1/2, 1/3)$ ,  $C = (1/6, 2/3, 1/6)$  and  $D = (1/3, 1/2, 1/6)$ . Then  $2AB^2 + 2BC^2 = 4.34$  but  $AC^2 + BD^2 = 3.8436241135$ .

$\lambda$  of  $\mathbb{R}^d$ : Let  $B_p$  denote the unit ball wrt. to the Finsler norm at point  $p \in \mathcal{C}$ , and  $B_e$  the Euclidean unit ball. Then the Busemann measure for a Borel set  $\mathcal{B}$  is defined by [82]:

$$\mu_{\mathcal{C}}(\mathcal{B}) = \int_{\mathcal{B}} \frac{\lambda(B_e)}{\lambda(B_p)} d\lambda(p).$$

The existence and uniqueness of center points of a probability measure in Finsler geometry have been investigated in [6].

## C Bounding Hilbert norm with other norms

Let us show that  $\|v\|_{\text{NH}} \leq \beta_{d,c} \|v\|_c$ , where  $\|\cdot\|_c$  is any norm. Let  $v = \sum_{i=0}^d e_i x_i$ , where  $\{e_i\}$  is a basis of  $\mathbb{R}^{d+1}$ . We have:

$$\|v\|_c \leq \sum_{i=0}^d |x_i| \|e_i\|_c \leq \|x\|_2 \underbrace{\sqrt{\sum_{i=0}^d \|e_i\|_c^2}}_{\beta_d},$$

where the first inequality comes from the triangle inequality, and the second inequality is from the Cauchy-Schwarz inequality. Thus we have:

$$\|v\|_{\text{NH}} \leq \beta_d \|x\|_2,$$

with  $\beta_d = \sqrt{d+1}$  since  $\|e_i\|_{\text{NH}} \leq 1$ .

Let  $\alpha_{d,c} = \min_{\{v : \|v\|_c=1\}} \|v\|_{\text{NH}}$ . Consider  $u = \frac{v}{\|v\|_c}$ . Then  $\|u\|_c = 1$  so that  $\|v\|_{\text{NH}} \geq \alpha_{d,c} \|v\|_c$ . To find  $\alpha_d$ , we consider the unit  $\ell_2$  ball in  $V^d$ , and find the smallest  $\lambda > 0$  so that  $\lambda B_V$  fully contains the Euclidean ball.

Therefore, we have overall:

$$\alpha_d \|x\|_2 \leq \|v\|_{\text{NH}} \leq \sqrt{d+1} \|x\|_2$$

In general, note that we may consider two arbitrary norms  $\|\cdot\|_l$  and  $\|\cdot\|_u$  so that:

$$\alpha_{d,l} \|x\|_l \leq \|v\|_{\text{NH}} \leq \beta_{d,u} \|x\|_u.$$

## D Funk directed metrics and Funk balls

The Funk metric [68] wrt a convex domain  $\mathcal{C}$  is defined by

$$F_{\mathcal{C}}(x, y) = \log \left( \frac{\|x - a\|}{\|y - a\|} \right),$$

where  $a$  is the intersection of the domain boundary and the affine ray  $R(x, y)$  starting from  $x$  and passing through  $y$ . Correspondingly, the reverse Funk metric is

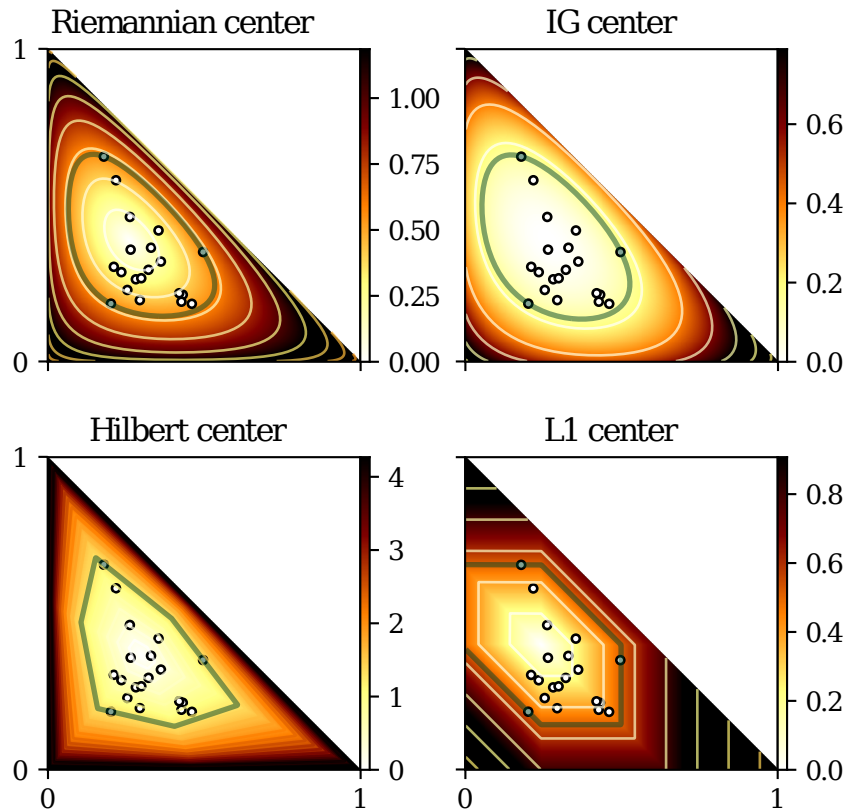
$$F_{\mathcal{C}}(y, x) = \log \left( \frac{\|y - b\|}{\|x - b\|} \right),$$

where  $b$  is the intersection of  $R(y, x)$  with the boundary. The Funk metric is *not* a metric distance.

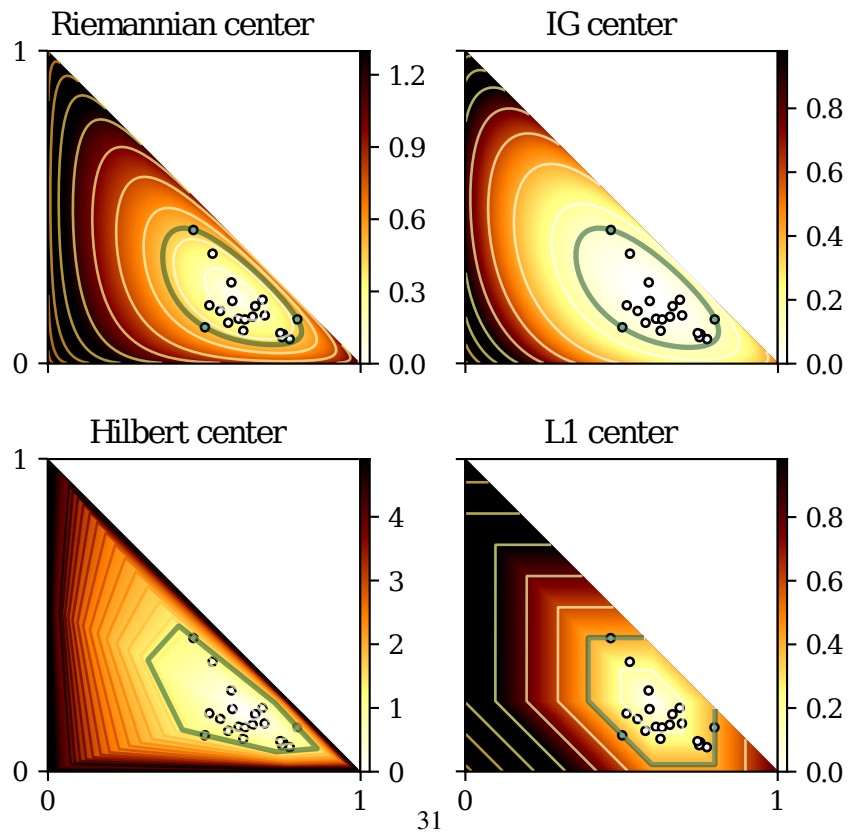
The Hilbert metric is simply the arithmetic symmetrization:

$$H_{\mathcal{C}}(x, y) = \frac{F_{\mathcal{C}}(x, y) + F_{\mathcal{C}}(y, x)}{2}.$$

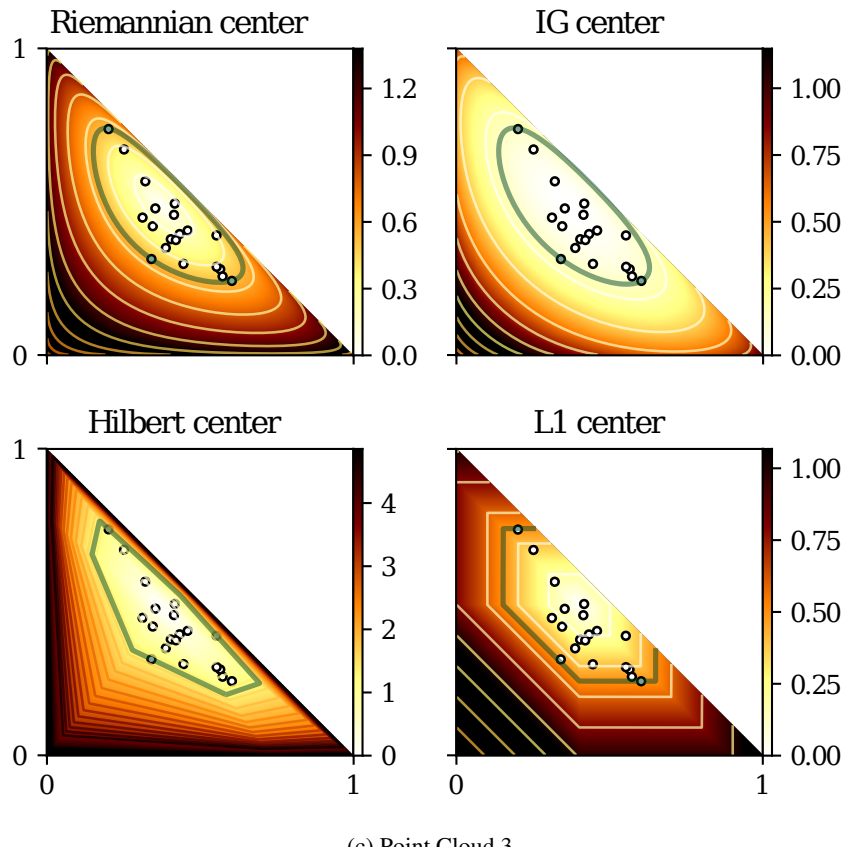
It is interesting to explore clustering based on the Funk geometry, which we leave as a future work.



(a) Point Cloud 1



(b) Point Cloud 2



(c) Point Cloud 3

Figure 13: The Riemannian/IG/Hilbert/ $L_1$  minimax centers of three point clouds in  $\Delta^2$  based on Alg. (4). The color maps show the distance from  $\forall p \in \Delta^2$  to the corresponding center.

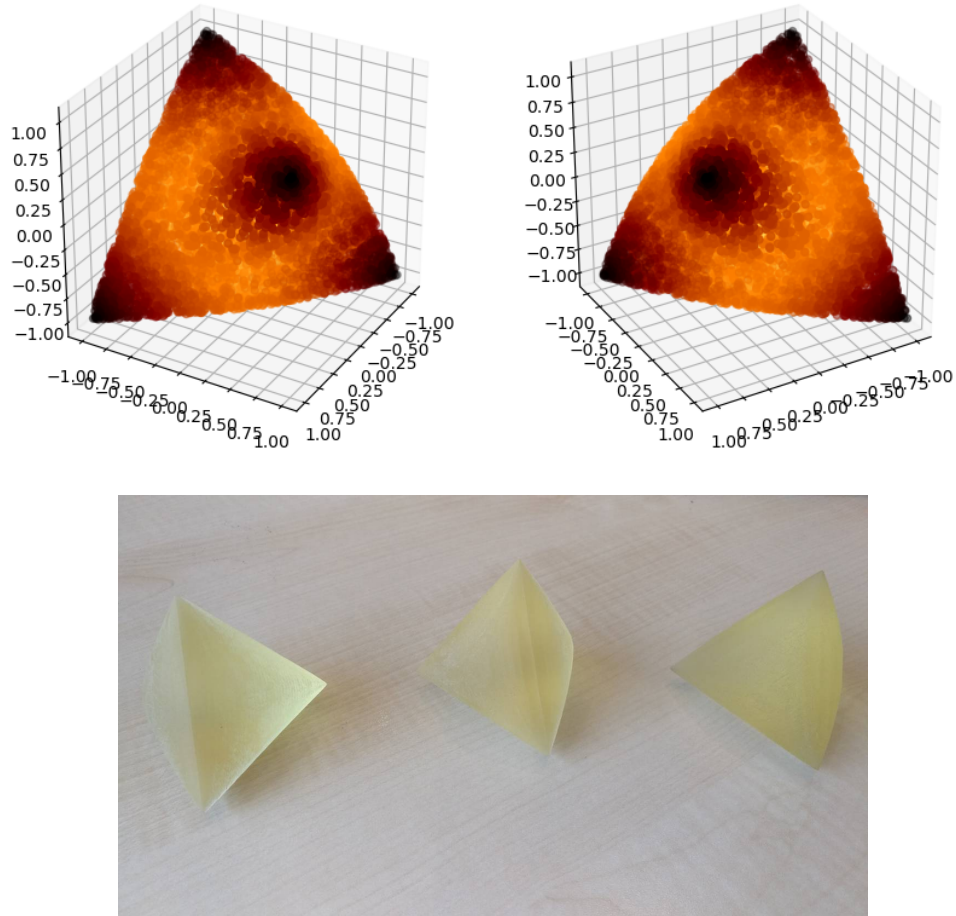


Figure 14: The ellotope  $\mathcal{C}_3$  (two different perspectives), and three 3D printed elliptopes.

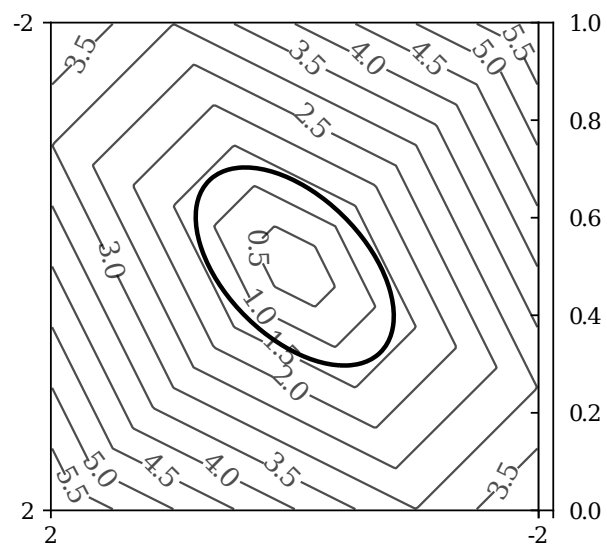


Figure 15: Polytope balls  $B_V$  and the Euclidean unit ball  $B_E$ . From the figure the smallest polytope ball has radius  $\approx 1.5$ .